1   **Bromodomain factor 5 is an essential transcriptional regulator of the *Leishmania* genome.**

2

3   Nathaniel G. Jones[1*], Vincent Geoghegan[1], Gareth Moore[1], Juliana B. T. Carnielli[1], Katherine

4   Newling[1], Félix Calderón[2], Raquel Gabarró[2], Julio Martín[2], Rab Prinjha[3], Inmaculada Rioja[3],

5   Anthony J. Wilkinson[4], Jeremy C. Mottram[1].

6

7   1: York Biomedical Research Institute and Department of Biology, University of York, United

8   Kingdom

9

10   2: GlaxoSmithKline Global Health, Tres Cantos, 28760, Madrid, Spain

11

12   3: Immunology Research Unit, Research, R&D GlaxoSmithKline, Gunnels Wood Road,

13   Stevenage, Herts, SG1 2NY, UK

14

15   4: York Biomedical Research Institute and York Structural Biology Laboratory, Department of

16   Chemistry, University of York, United Kingdom

17

18   *Corresponding author.

19

22

23   **Abstract**

24   *Leishmania* are unicellular parasites that cause human and animal disease. Alongside other

25   organisms in kinetoplastida, they have evolved an unusual genome architecture that requires

26   all RNA polymerase II transcribed genes to be expressed constitutively, with transcriptional

27   start regions denoted by histone variants and histone lysine acetylation. However, the way

28   these chromatin marks are interpreted by the cell is not understood. Seven predicted

29   bromodomain factors (BDF1-7), the reader modules for acetyl-lysine, were identified across

30   *Leishmania* genomes. Using *L. mexicana* as a model, Cas9-driven gene deletions indicate that

31   BDF1-5 are essential for promastigote survival, whilst DiCre inducible gene deletion of the

32   dual bromodomain factor *BDF5* identified it to be essential for both promastigotes and

33   amastigotes. ChIP-seq assessment of BDF5s genomic distribution revealed it as highly

34   enriched at transcriptional start sites. Using an optimised proximity proteomic and

35   phosphoproteomic technique, XL-BioID, we defined the BDF5-proximal environment to be

36   enriched for other bromodomain factors, histone acetyltransferase 2, and proteins essential

37   for transcriptional activity and RNA processing. Inducible deletion of BDF5, led to a disruption

38   of pol II transcriptional activity and global defects in gene expression. Our results indicate the

39   requirement of *Leishmania* to interpret histone acetylation marks for normal levels of gene

40   expression and thus cellular viability.

41

Introduction

Gene transcription in eukaryotic cells is a complex process with multiple levels of regulation[1]. Post-translational modifications (PTMs) of histones in nucleosomes can be used to encode an extra layer of information into chromatin, to modify transcriptional activity leading to differential gene expression. Histone modification by lysine acetylation is one predominant modification, it is interpreted by 'reader' proteins called bromodomains. In eukaryotic pathogens such as *Leishmania*, an organism with an unusual genome arrangement, the impact of histone lysine acetylation on transcriptional regulation is not well understood.

Bromodomains are small protein domains consisting of 100-110 amino acid residues folded into a bundle of 4 helices connected by two loops which form a hydrophobic pocket that can bind to acetyl-lysine modified peptides. Conserved tyrosine and asparagine residues serve as acetyl-lysine recognition elements along with a network of water molecules in the pocket [2–4]. Bromodomains are classically found to recognise acetyl-lysine residues of histone tails, allowing bromodomain-containing proteins to act as interpreters of the histone acetylation code. Proteins containing bromodomains are often called bromodomain factors (BDFs). Other accessory domains in the BDF or its binding partners can then conduct other functions such as applying additional PTMs or chromatin remodelling. BDFs can regulate processes at specific regions of genomes such as promoters or enhancers, influencing differential gene expression, leading to cellular proliferation or differentiation. Inhibitors of these interactions have been intensely explored to identify pharmacological interventions for diseases driven by dysregulated BDF-driven processes [3–6].

Bromodomain proteins are poorly studied in kinetoplastid species, such as *Leishmania*, the causative agents of multiple human and animal diseases. Visceral leishmaniasis infects 50, 000 – 90, 000 people per year and the cutaneous forms of the disease, including those caused by *L. mexicana*, afflict up to 1 million people per year[7]. Kinetoplastids are deeply branched eukaryotes and their gene expression is radically different to the human host[8]. Genes are arranged into unidirectional polycistronic transcription units (PTU) of hundreds of non-functionally linked genes, and expression is driven from vaguely defined transcriptional start sites (TSS) that are often thousands of bases long[9]. The PTUs can run on either the plus or minus strand from transcriptional start sites at divergent strand switch regions[10]. Where PTUs then meet, a convergent SSR occurs, these are transcriptional termination sites (TTS). During transcription of protein-coding genes, RNA polymerase II (pol II) generates polycistronic pre-mRNAs that are processed by co-transcriptional cleavage, polyadenylation and trans-splicing events to produce mature mRNAs. Expression levels of individual genes are then typically regulated by the 3' UTR, which is targeted by RNA binding proteins for stabilisation, sequestration or degradation[11]. In *Leishmania,* some highly expressed genes are found in tandem arrays or on supernumerary chromosomes to increase gene dosage[12]. *Leishmania* also exhibit high levels of mosaic aneuploidy in cell populations as an adaptive survival

83   strategy allowing plastic variation in gene dose[13]. Consequently, transcription of protein-
84   coding genes by polymerase II was thought to be constitutive with no sequence-defined,
85   promoter-specific regulation[14]. However, it appears that cellular demarcation of
86   transcriptionally start sites might be mediated through histone acetylation to provide a
87   platform of accessible chromatin. This suggestion comes from the identification of H3
88   acetylation at TSSs in *L. major*[14]. Histone acetyltransferases have been identified as essential
89   for *L. donovani* survival and linked to specific histone modifications[15–18].

90

91   *Leishmania* is particularly poorly understood in terms of its transcriptional regulation by
92   acetylation; however, because of the high level of synteny and conservation of their genomic
93   features to *Trypanosoma,* some of their core epigenetic processes may also be conserved.
94   TSSs in *Trypanosoma brucei* are enriched for histone variants and acetylation marks[19], the
95   number of different histone PTMs in *T. brucei* has been shown to range into the hundreds
96   [20,21]. Recently, characterisation of chromatin-associated proteins in *T. brucei* led to the
97   identification of specific networks of bromodomain factors and other proteins at TSS and TTS,
98   with characteristic ChIP-seq profiles suggesting a specific ordering and unexpected
99   complexity of processes at these sites[22]. It has been reported that after genetic or chemical
100   targeting of TbBDF2 and TbBDF3 in bloodstream stage *T. brucei*, cells undergo a process
101   consistent with aberrant differentiation to the insect stage forms, identifying a potential role
102   in the lifecycle of the parasite[23]. Several BDFs have been shown to be essential in multiple life
103   stages of *T. brucei* by using a genome-wide RNAi screen[24]. TbBDF5 has been individually
104   targeted by RNAi in bloodstream forms and found to be essential for cellular survival[25]. In
105   *Trypanosoma cruzi* bromodomain factors TcBDF1 and TcBDF3 have been implicated in cellular
106   differentiation, intriguingly TcBDF1 has been reported to localise to glycosomes and TcBDF3
107   has been reported to interact with acetylated tubulin in the flagellum[26–28]. TcBDF2 has been
108   reported to bind acetylated histone $TcH4K10_{ac}$ and accumulates in cells treated with UV
109   radiation[29]. Until now, none of these orthologs have been characterised in *Leishmania.*

110

111   In this work, we validate five bromodomains factors as essential in *Leishmania* and
112   characterise the biology co-ordinated by the essential bromodomain factor, BDF5. By
113   applying inducible gene deletion, we were able to establish the requirement for BDF5 in both
114   cell culture and a mammalian host. We applied multiple -omics tools to characterise the
115   function of BDF5, in particular using ChIP-seq to define the genomic distribution of BDF5,
116   proximity proteomics to determine the processes occurring in BDF5-enriched loci and RNA-
117   seq to explore the role of BDF5 in gene expression. Integrating the findings of these
118   approaches we defined BDF5 as an essential factor required for pol II transcriptional activity
119   in *Leishmania*.

120

121

Results

Bromodomain factors in Leishmania
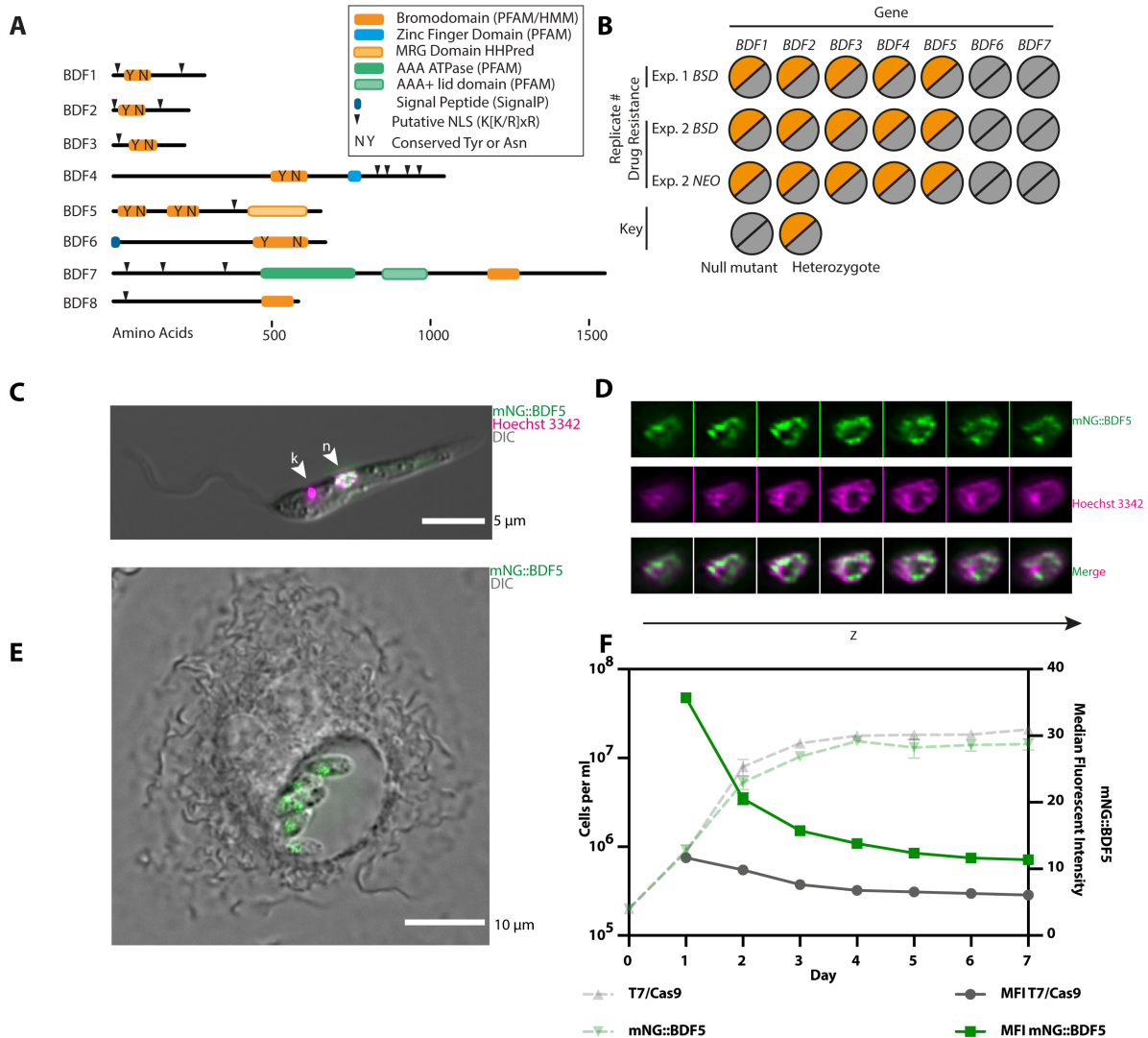
Figure 1: **Overview of putative *Leishmania* bromodomain factors. A**. Schematic showing protein domain architecture of *Leishmania* BDFs. **B**. Overview of Cas9 gene deletion attempts of *BDF1-7* in *L. mexicana T7/Cas9* promastigotes. Two independent transfections were carried out using either *BSD* or *NEO* as a drug selectable marker individually or in combination. **C**. Live-cell fluorescent microscopy of *L. mexicana* promastigote expressing mNG::BDF5. Nucleus is denoted by arrowhead labelled n, the kinetoplastid DNA is indicated by arrowhead labelled k. **D**. Channel separated Z-slices of the nucleus from the cell in (C). **E**. Live-cell fluorescent microscopy of intra-macrophage *L. mexicana* amastigotes expressing mNG::BDF5 endogenously-tagged protein. **F**. Expression levels of mNG::BDF5 during promastigote growth, determined by mNG signal in individual cells by flow-cytometry. Dashed points denote mean cell density, error bars ± standard deviation, solid points denote median fluorescence intensity, N=3, 20, 000 events per sample.

Although bromodomain factors BDF1-5 were readily identifiable in *Leishmania* genomes[30], further PFAM and HMM searching identified another two potential bromodomain-containing proteins BDF6 and BDF7 (**Fig. 1A, Table 1**) (Tallant, C, et al. In Press doi;.

141   10.1021/acsinfecdis.1c00387). BDF1-5 have identifiable tyrosine and asparagine residues in
142   positions consistent with the conserved residues important for peptide binding in canonical
143   bromodomains. BDF1-3 are small proteins <500 residues and contain a single bromodomain
144   and no other identifiable domains. BDF4 is a larger protein with a centrally located
145   bromodomain followed by a predicted CW-type zinc finger. BDF5 is the only *Leishmania* BDF
146   that has tandem bromodomains in the N-terminal half of the protein. We refer to these as
147   BD5.1 and BD5.2 and both are located in the N-terminal half of the protein. A more sensitive
148   HHPred[31] analysis suggested remote structural homology to an MRG domain-like region
149   (MORF4 (mortality factor on chromosome 4) related gene) in the C-terminal half of the BDF5
150   protein. MRG domains can bind transcriptional regulators and chromatin remodelling
151   factors[32–34]. BDF6 and BDF7 contain the most divergent bromodomains. BDF6 includes an
152   insert in the bromodomain region and BDF7 lacks the conserved tyrosine and asparagine
153   residues, suggesting that they may be divergent, noncanonical bromodomains or pseudo-
154   bromodomains[35]. BDF6 has a C-terminal bromodomain and is predicted to have an N-terminal
155   signal peptide when analysed using SignalP4.1. BDF7 is the largest of the BDFs and contains a
156   bromodomain in the C-terminal region of the protein preceded by a predicted ATPase and
157   AAA domain. The bromodomain does not appear to have the conserved tyrosine and
158   asparagine residues that are important for acetyl-lysine binding. However, by HMMER
159   analysis and alignment, it appears that BDF7 might be a homologue of the ATAD2 factor found
160   in many other eukaryotes[36–38]. All of the predicted BDFs, apart from BDF6, contain
161   K[K/R]x[K/R] motifs that can act as a monopartite nuclear localisation signal[39]. The BDFs of
162   *Leishmania* have orthologs in other parasitic and free-living kinetoplastid organisms, except
163   for BDF1 in *Bodo saltans* [40,41]. BDF8 was identified by HHPred analysis of a hypothetical gene
164   identified using BDF5-proximity proteomics (this study), it may represent another pseudo-
165   bromodomain.
166
167   To assess the essentiality of the seven BDFs in *Leishmania* promastigotes we used Cas9-
168   targeted gene deletion. sgRNAs and repair templates were generated to target the CDS of
169   each gene and replace it completely (**Fig. S1A**)[42]. Two independent experiments were
170   performed, using either blasticidin (*BSDI* or *BSD* and neomycin (*NEO*) drug resistance repair
171   cassettes, leading to three semi-independent selections. Consistently, BDF6 and BDF7 null
172   mutants could be isolated (**Fig. 1B, Fig. S1B, S1C, S1D**). For BDF1-5 only heterozygote mutants
173   were ever isolated, indicating that although the Cas9 system was functioning, a copy of the
174   gene was required for promastigote survival and thus null mutants could not be generated.
175
176   LmxBDF5, while distinct from BET bromodomains, shares a characteristic tandem
177   bromodomain arrangement reminiscent of human BRD2 and BRD4, or the yeast RSC4
178   protein[4]. These proteins have all been identified to play roles in regulating transcription, so
179   due to this interesting feature of BDF5 we decided to investigate it in greater detail. BDF5
180   homologs are identifiable in all the kinetoplastid genomes available in TriTrypDB. The level of
181   amino acid conservation across the first bromodomain (BD5.1) is higher than the second

182   (BD5.2), but in all cases the conserved tyrosine and asparagine residues are retained in both
183   bromodomains (**Fig. S2A**), these correspond to Y40, N90, Y201 and N247 in LmxBDF5. Both
184   bromodomains have x-ray crystal structures available in the PDB (PDB ID: 5TCM, 5TCK),
185   confirming the bromodomain structural fold and positioning of conserved residues (**Fig. S2B**).
186   BDF5 was endogenously tagged using a Cas9 targeted approach to append a 3xMyc epitope
187   and the green fluorescent protein mNeonGreen to the N-terminus[42] to generate *mNG::BDF5*.
188   This modification preserves the 3' UTR, which is necessary for regulating endogenous mRNA
189   levels in *Leishmania* allowing for native expression levels and dynamics through growth and
190   lifecycle stages. Live-cell widefield deconvolution microscopy of promastigotes identified that
191   mNG::BDF5 localised to the nucleus (**Fig. 1C**). The distribution of mNG::BDF5 within the
192   nucleus was heterogeneous, with foci found around the periphery of the nucleus and
193   excluded from the nucleolus (**Fig. 1D**). The expression of mNG::BDF5 persisted in amastigotes
194   where it was visualised in a structure consistent with the nucleus of intramacrophage
195   amastigotes (**Fig. 1E**). *BDF5* mRNA was also previously detected to be constitutively expressed
196   in both lifecycle stages[43]. A seven-day time course experiment was performed where
197   mNG::BDF5 levels in individual cells were measured by flow cytometry to determine the
198   levels of BDF5 during promastigote growth (**Fig. 1F**). mNG::BDF5 levels were highest in rapidly
199   proliferating cells during the first few days of growth and declined as the cells approached
200   stationary phase. By day 7, mNG::BDF5 levels were reduced by >60% compared to day 2.
201   mNG::BDF5 signal was not completely reduced to the levels of the parental control strain,
202   suggesting a low level of BDF5 expression was retained.
203
204   **Table 1: Gene IDs for *L. mexicana* BDFs and orthologues in selected trypanosomatids.** PDB
205   identifiers are provided for available structures, shaded boxes represent likely pseudo-
206   bromodomains.

Name	*L. mexicana* gene	*L. donovani gene*	PDB ID	*T. brucei* orthologue	PDB ID	T. cruzi orthologue	PDB ID
BDF1	LmxM.36.6880	LdBPK_367210.1		Tb927.10.8150	5KO4	TcCLB.506247.80	
BDF2	LmxM.36.2980	LdBPK_363130.1	5C4Q	Tb927.10.7420	4PKL, 5CZG, 2N9G	TcCLB.507769.30	6NP7, 6NIM
BDF3	LmxM.36.3360	LdBPK_363520.1	5FEA	Tb927.11.10070	5C8G	TcCLB.509747.110	
BDF4	LmxM.14.0360	LdBPK_140360.1		Tb927.7.4380		TcCLB.508857.150	
BDF5	LmxM.09.1260	LdBPK_091320.1	5TCM, 5TCK	Tb927.11.13400	5K29, 6NEZ	TcCLB.510359.130	6NEY
BDF6	LmxM.12.0430	LdBPK_120390.1		Tb927.1.3400		TcCLB.510889.330	
BDF7	LmxM.11.0910	LdBPK_110910.1		Tb927.11.6350		TcCLB.506297.110	
BDF8	LmxM.33.2300	LdBPK_342070.1		Tb927.4.2340		TcCLB.506559.310	

207
208
209

BDF5 is essential in promastigotes and for murine infection
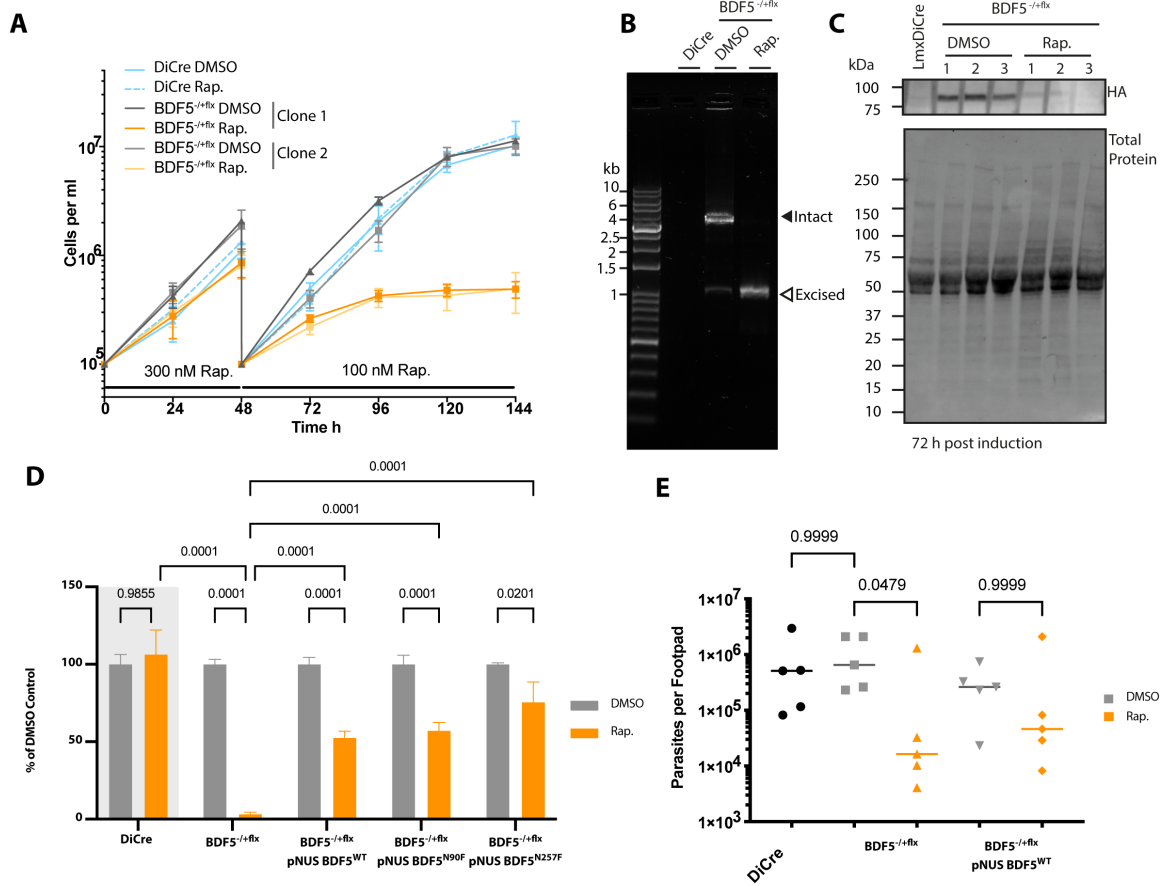
Figure 2: Characterisation of inducible knockout of BDF5 using DiCre. **A**. Growth curve of promastigotes treated with the inducing agent, rapamycin (Rap.), or the vehicle, DMSO. Points and error bars denote mean values ± standard deviation, n=3. **B**. PCR and agarose gel analysis of *BDF5::6xHA*^{flx} gene excision at the 72 h timepoint in (A). Solid arrowhead denotes the intact *BDF5::6xHA*^{flx} gene and open arrowhead denotes the excised locus after rapamycin addition. The DiCre lane indicates the lack of PCR product in the parental strain. **C**. Western blot showing levels of BDF5::6xHA protein at the 72 h timepoint. **D**. Results of clonogenic survival assay comparing BDF5 depleted cells with cell lines carrying episomal complementation of *BDF5* or mutated *BDF5* alleles. Bars denote the mean of the percentage clonal survival where each experiment was normalised to its own DMSO control. Error bars indicate standard deviation, values above are p values from 2-way ANOVA with multiple comparisons by Tukey's test, n=3. Lines denote comparisons performed by two-way ANOVA with associated p-values shown above **E**. Parasite burdens from infected mouse footpads determined by limiting dilution, individual points for each mouse with median values indicated by lines. Comparisons of Kruskal-Wallace test with Dunn's correction indicated with associated p-values written above, n=5.

To gain a higher quality validation of *BDF5* essentiality[44] and to investigate the phenotypes resulting from loss of BDF5 in promastigotes, an inducible knockout strain was generated using the DiCre system[45,46] (**Fig. S2A, S2B**). An *L. mexicana* strain expressing dimerisable, split Cre recombinase was modified to carry a single, 6xHA epitope-tagged allele of *BDF5* flanked by loxP sites giving *L.mx::DiCre Δbdf5::BDF5::6xHA*^{flox}*/BDF5.* The second copy of BDF5 was

234 then deleted using a *HYG* resistance cassette giving the strain
235 *L.mx::DiCreΔbdf5::HYG/Δbdf5::BDF5::6xHA^{flox}*, referred to as *BDF5::6xHA^{-/+flx}*. In the absence
236 of rapamycin, this strain grew normally as per the parental DiCre strain. However, following
237 the addition of rapamycin, there was a marked reduction in the parasite growth (**Fig. 2A**).
238 Rapamycin was added to cultures at 300 nM for 48 h at which point the cultures were diluted
239 to 1 x 10^5 cells per ml. Rapamycin was then added at 100 nM to suppress escape mutants
240 and the growth phenotype observed. At the 144 h time point, the rapamycin-treated flasks
241 contained ~98% fewer cells than the controls. Rapamycin did not affect the parental DiCre
242 strain, indicating that the effect was specific to the floxed strain where *BDF5* could be deleted.
243 This phenotype was reproducible and observed in an independent, clonal cell line (**Fig. 2A**).
244 PCR analysis of these populations at 72 h after rapamycin addition revealed that the
245 *BDF5::6xHA^{flx}* allele had been excised (**Fig. 2B**). Some leaky excision of the *BDF5::6xHA^{flx}* allele
246 was detectable in the untreated control samples. The levels of BDF5::6xHA protein at 72 h
247 were assessed by western blot, revealing a 90% reduction in the rapamycin-treated sample
248 compared to the control samples (**Fig. 2C**). Total protein Stain-Free technology was used to
249 provide loading controls, due to the potential for BDF5 deletion to impact on transcription of
250 housekeeping genes. To demonstrate that the deletion of *BDF5* was essential for cellular
251 survival a clonogenic assay was applied to characterise the cells resulting from *BDF5* excision
252 (**Fig. 2D**). A 98% reduction in survival of the *BDF5::6xHA^{-/+flx}* strain was observed when cloned
253 in the presence of 100 nM rapamycin, moreover, those cells that survived retained the
254 *BDF5::6xHA^{flox}*allele.

255

256 To ensure the phenotype was specific to *BDF5* deletion and not due to off-target effects, an
257 allele of *BDF5::GFP* was re-introduced to the *BDF5::6xHA^{-/+flx}* strain using the pNUS episome[47]
258 (**Fig. S4**) Clonal survival experiments were performed in media lacking drug selection for the
259 episome allowing for its loss if it confers no selective advantage. Clonal survival of the BDF5-
260 complementation strain was ~50% after rapamycin addition, this is 25-fold higher than the
261 non-complemented, induced samples. While not 100% complementation it reflects the
262 potential for parasites to lose the episome (**Fig. 2D**), demonstrating the requirement for BDF5
263 for cellular survival. This experimental approach also allowed us to explore the essentiality of
264 the individual bromodomains by making point mutations at the conserved asparagine
265 residues in each bromodomain, N90 and N257 in BD5.1 and BD5.2 respectively (**Fig. S4**). These
266 were mutated to phenylalanine in anticipation that the bulky sidechain would displace any
267 binding peptide from the hydrophobic pocket[2,48,49]. Clonal survival was restored to similar
268 levels as those observed for the *pNUS BDF5* complementation strain by the *BDF5^{N90F}* and
269 *BDF5^{N257F}* mutants (**Fig. 2D**), indicating that either these mutations are not disruptive, or that
270 any disruption due to mutation of a single BDF5 BD is tolerated by the cell. Three attempts
271 were made to generate double mutations in N90F/N257F but no viable populations of cells
272 were isolated, suggesting the *BDF5^{N90F/N257F}* is not tolerated by the cells. In light of this, we
273 used a DiCre inducible system[50] to flip-on expression of an extra *BDF5^{N90F/N257F}::GFP* mutant
274 allele to look for dominant-negative phenotypes (**Fig. S5A, Fig.S5B**). Promastigote cultures

275   induced to express BDF5$^{N90F/N257F}$::GFP exhibited a significant growth defect (**Fig. S5C, S5D**),

276   whereas those induced to express the BDF5::GFP protein did not exhibit this phenotype.

277   These experiments demonstrate that individually both bromodomains are redundant, but

278   that together they are required for the essential function of BDF5.

279

280   The ability to use the DiCre strains to validate target genes in *Leishmania* amastigotes is

281   restricted due to the toxicity of rapamycin to amastigotes and its immunomodulatory effect

282   in mammals[45]. Therefore, mid-log promastigote cultures of *Lmx::DiCre*, *BDF5::6xHA$^{-/+flx}$* or

283   *BDF5::6xHA$^{-/+flx}$ ::pNUS BDF5::GFP* were treated with 500 nM rapamycin or DMSO for 72 hours

284   allowing them to induce deletion of BDF5 but still allow infectious, metacyclic promastigotes

285   to accumulate in culture. Excision of the BDF5 gene was verified by PCR (**Fig. S6A**) and the

286   stationary cultures were used to infect BALB/c mice by a subcutaneous route into the rear

287   footpad. No apparent differences were observed in the size of the resulting footpad lesions

288   over the 8-week infection period (**Fig. S6B**), however, there was a 50-fold reduction in the

289   parasite burden of the footpads when infected with *BDF5::6xHA$^{-/+flx}$* rapamycin treated cells

290   compared to the *BDF5::6xHA$^{-/+flx}$* DMSO treated cells or the parental strain (**Fig. 2E**). The

291   presence of the *pNUS BDF5::GFP* episome restored parasite burden in the rapamycin-treated

292   strain to a level not significantly different to that observed in its uninduced control (**Fig. 2E**).

293   The median parasite burdens of the *BDF5::6xHA$^{-/+flx}$* strain rapamycin-treated strain in the

294   popliteal lymph nodes was ~10-fold lower than the control strain, but this difference was not

295   statistically significant (**Fig. S6C**). DNA extracted from footpads and lymph nodes, including

296   both host and amastigote DNA, was subjected to PCR analysis which detected non-excised

297   BDF5::6xHA$^{-/+flx}$ consistent with BDF5 being essential for amastigote survival as well as

298   promastigote survival (**Fig. S6D**). Clonal promastigote lines lacking the *BDF5::6xHA$^{-/+flx}$* allele

299   could only be derived from the populations containing an addback copy of BDF5 (**Fig. S6E**).

300   We conclude that BDF5 is essential for successful infection of the mammalian host and is likely

301   to be essential for amastigote survival too.

302

303   *ChIP-seq reveals BDF5 genomic distribution*
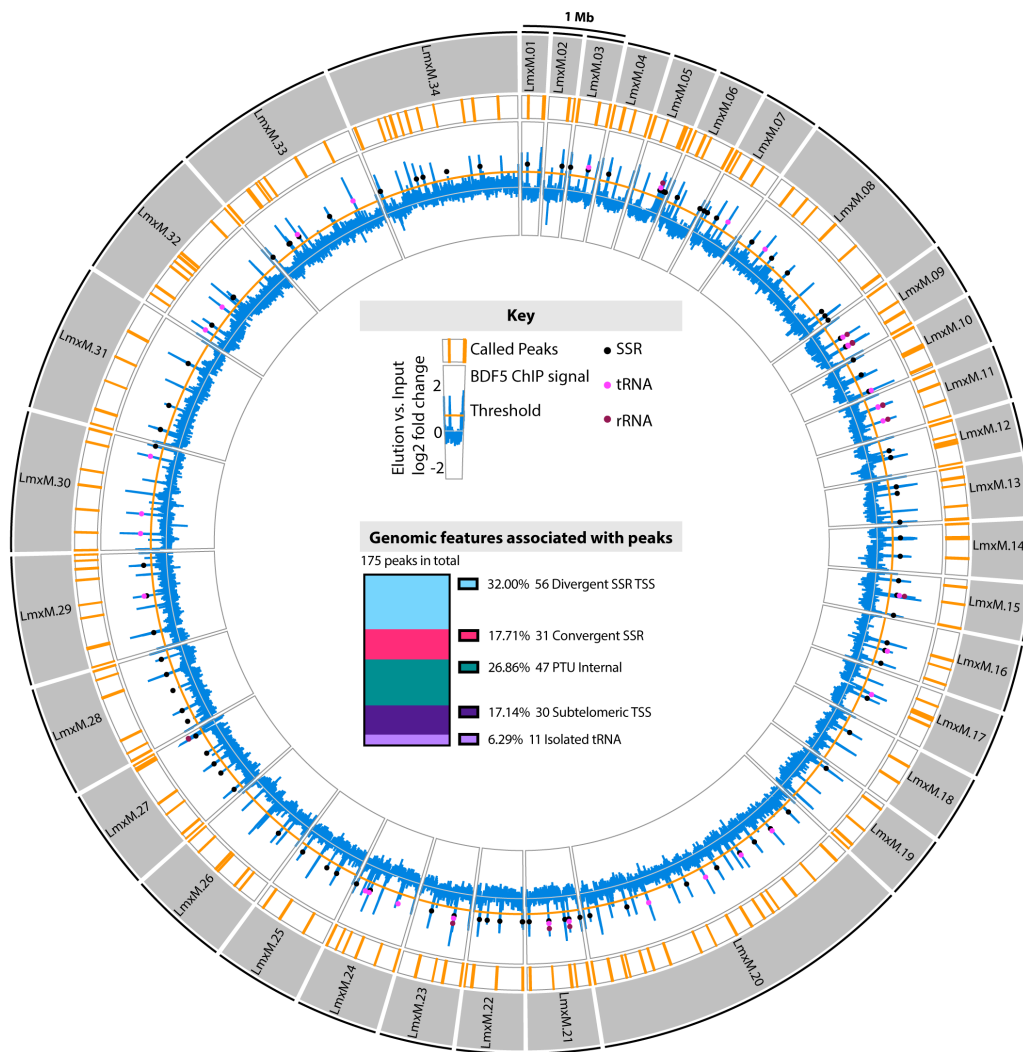
304

305

306   Figure 3: **Genome-wide distribution of BDF5 determined by ChIP-seq analysis.** Outer circles:
307   Circos plot representing the 32 MB *L. mexicana* genome. The 34 chromosomes are depicted
308   by grey segments. Regions enriched >0.5 log2fold for BDF5 indicated by the orange bars, the
309   enrichment of BDF5::6xHA in the elution over the input chromatin is indicated in the blue line
310   on a log2 fold scale, values are the mean derived from 3 ChIP replicates. Genomic features
311   such as strand-switch regions, tRNA genes, and rRNA genes are indicated by coloured circles
312   on this blue line. Inner pane: Key and stacked bar chart showing the genomic features
313   associated with the peaks.

314

315   Due to the importance of BDF5 for the survival of *Leishmania* parasites and the demonstration
316   that it is a nuclear protein, we sought to identify where it might be found in the context of
317   genomic architecture. The BDF5::6xHA protein expressed by the *BDF5::6xHA^{-/+flx}* strain was
318   analysed by chromatin immunoprecipitation sequencing (ChIP-Seq). We identified 175
319   regions where BDF5 was determined to be enriched on the genome; these peaks were
320   distributed across all the 34 chromosomes and could be correlated with specific genomic
321   features (**Fig. 3, Fig. S7A, S7B**). Of the total peaks, 56 (32%) were associated with TSSs in

322   divergent strand switch regions (dSSRs). A further 30 (17%) were in subtelomeric regions likely

323   to be transcriptional start sites based on the orientation of the polycistronic transcription

324   unit. Forty-seven peaks (27%) were identified in internal regions of polycistronic transcription

325   units (PTUs) and a further 11 peaks overlapped with isolated tRNA genes (6%). Intriguingly,

326   31 peaks (18%) were found at convergent strand switch regions, which are likely

327   transcriptional termination sites. The size of the regions determined to be enriched for BDF5

328   varied, with the mean of peaks found at dSSRs encompassing ~10 kb (**Fig. S7C**). The shape of

329   BDF5 peaks over divergent strand switch regions tended to be broad and even, without

330   exhibiting the "twin-peaks" pattern seen for histone H3 acetylation in *L. major*[14] (**Fig. S7A,**

331   **S7D**). Peaks at both divergent and convergent SSRs tended to be symmetrical although they

332   were narrower and weaker at convergent SSRs (cSSRs) (**Fig. S7D**). Peaks found in PTUs were

333   asymmetric, rising steeply to a peak with a shallow decay in the direction of the PTU

334   transcription. The PTU peak enrichment levels were equivalent to those at dSSRs (**Fig. S7E**).

335   The finding that BDF5 predominantly localises to divergent SSRs and other TSSs suggests it

336   plays a role in polymerase II transcription. However, as a number of termination sites and

337   other classes of small RNA genes were also enriched for BDF5 this indicates it could also play

338   a generalised role in a range of transcriptional processes. Therefore, we sought to analyse the

339   protein complexes associated with BDF5 to give insight into its potential function.

340

341

342

343

344

345

346

347

348

349

350

351

352

353

354

355   *XL-BioID identifies the BDF5 proximal proteome*
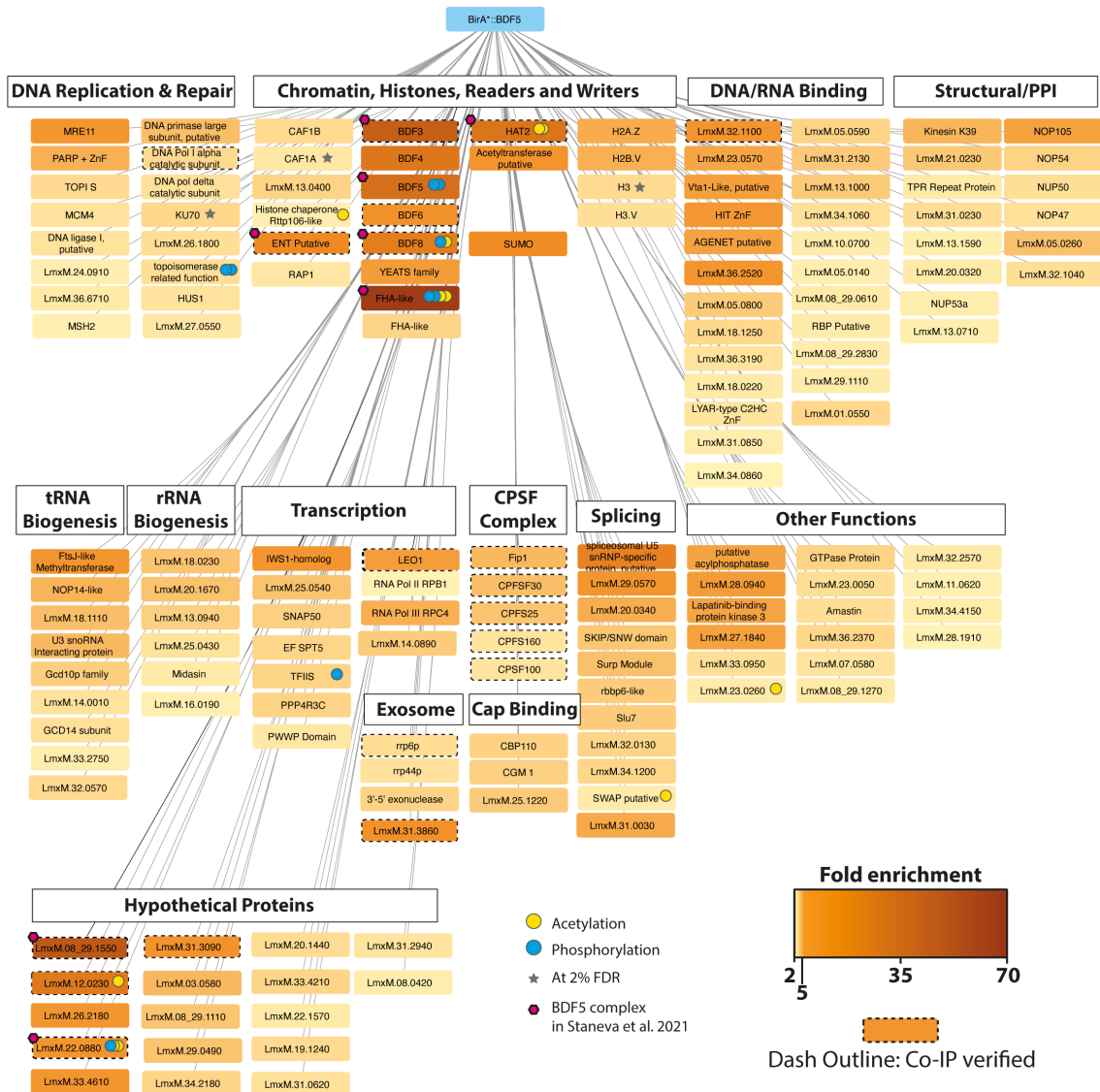
Figure 4: The BDF5-proximal proteome determined by XL-BioID. Network indicates proteins determined to be spatially enriched in proximity to BirA*::BDF5 following biotin labelling and DSP cross-linking. Fold enrichment values are encoded in the colour intensity of the protein boxes; these were calculated from label free protein intensities against a control expressing KKT19::BirA*, from 3 replicate experiments. A dashed outline to a box indicates that BDF5 co-purified with this protein in a reciprocal co-immunoprecipitation experiment. If a post translational modification (PTM) was detected for a protein, this is indicated using a coloured circle. Proteins are grouped by functional annotations or previously published data of complexes in *Leishmania* or *Trypanosoma*. Proteins represented are those identified at 1% false-discovery rate (FDR), those marked with a grey star denote those identified at 2% FDR for select proteins. CPSF stands for cleavage and polyadenylation specificity complex, PPI stands for protein-protein interactions. Magenta hexagons indicate members of the BDF5, BDF3, HAT2 complex reported in *T. brucei*.

To identify the functional properties of the environment proximal to BDF we applied an in-situ proximity labelling technique, cross-linking BioID (XL-BioID)[51]. The promiscuous biotin ligase BirA*, which generates a locally reactive (~10 nm) biotinoyl-5'-AMP[52], was fused to the

374   N-terminus of BDF5 by endogenous tagging. The resultant parasites were incubated with 150
375   µM biotin for 18 h to permit labelling of proteins in proximity to BirA*::BDF5. The parasites
376   were then treated with a limited amount of dithiobis(succinimidyl propionate) (DSP) chemical
377   cross-linker, to increase the capture of proximal proteins which enriched with streptavidin,
378   trypsin digested and processed for LC-MS/MS analysis. Importantly, a control cell line was
379   treated in the same way to provide a control dataset of spatially segregated, nuclear proteins.
380   The nuclear-localised protein kinase KKT19[53] was chosen as it is expressed at similar levels to
381   BDF5 and localised to a distinct structure, the inner-kinetochore[54]. This provided a way to
382   subtract common background proteins labelled during the synthesis and trafficking of BDF5
383   to the nucleus as well as endogenously biotinylated cellular proteins. Following SAINTq
384   interaction scoring, 156 proteins were determined to be enriched at 1% FDR (**Fig. 4, Table
385   S2.**). A subset of these proteins was selected for endogenous tagging with 3xHA::mCherry in
386   mNG::BDF5 (which also contains a 3xmyc epitope) expressing strain to allow reciprocal co-
387   immunoprecipitation and verification of the XL-BioID dataset (**Fig. S8, Table S1**). This also
388   served to confirm there was no co-localisation of BDF5 and KKT19, and thus it was an
389   appropriate control protein.
390
391   The BDF5 proximal proteins were assessed for potential function (**Fig. 4**) and assembled into
392   a loose network. We identified a core set of 11 highly enriched proteins (>10-fold), including
393   the bait protein BDF5. Also identified were BDF3, BDF4 and Histone Acetyltransferase 2
394   (HAT2), along with several hypothetical proteins LmxM.35.2500, LmxM.08_29.1550,
395   LmxM.12.0230, LmxM.33.2300, LmxM.24.0530. A component of the spliceosome
396   LmxM.23.0650 was also identified, as was SUMO, which is likely conjugated to proteins in the
397   interactome (SUMO is a PTM common in the nucleus[55,56]). BDF5 was enriched 35-fold
398   compared to the control samples, BDF3 was enriched 41-fold and BDF4 26-fold. HAT2 was
399   enriched 27-fold, strongly suggesting that these proteins are in very close proximity and that
400   they may even form a stable complex. BDF6 (8-fold) and YEATS, a non-bromodomain acetyl-
401   lysine reader, (4.8-fold) were also identified, consistent with the chromatin environment
402   surrounding BDF5 being important sites of regulation through acetylation. The hypothetical
403   proteins of the interactome were assessed by Phyre2 and HHPRED for remote structural
404   homology to known domains that might indicate their function. LmxM.35.2500 was enriched
405   >65-fold compared to the control samples. HHpred analysis detected remote homology to
406   forkhead-associated domains, suggesting it may play a role in the recognition of
407   phosphorylation sites. LmxM.33.2300 was enriched 22-fold, HHPRED searching detected
408   remote structural homology related to bromodomains in the C-terminal region. However, it
409   appears to lack the conserved asparagine and tyrosine residues. LmxM.33.2300 may
410   therefore represent a degenerate bromodomain, therefore we propose to name it it BDF8.
411   LmxM.24.0530, which was enriched almost 14-fold, is predicted to contain an EMSY N-
412   Terminal Domain (ENT). EMSY is a protein implicated in DNA repair, transcription and human
413   tumorigenesis[57,58]. LmxM.24.1230 was identified as 7-fold enriched, and domain searching
414   identified a putative acetyltransferase in the N-terminal region as well as PHD-Zinc Finger

415   domain. Seventeen other enriched hypothetical proteins remained that lacked structural
416   homology to known protein domains.

417

418   Many proteins identified in the proximal proteome at lower enrichment levels play roles in
419   processes associated with active transcription, broadly separated into RNA transcription and
420   processing, including pre-mRNA cleavage, polyadenylation, splicing, cap-binding and quality
421   control (nuclear exosome), indicating that these processes are occurring in proximity to BDF5.
422   Components of RNA polymerase complexes were identified, including RPC4 associated with
423   RNA polymerase III, RPB1, the largest subunit of RNA polymerase II and the RNA polymerase-
424   associated protein LEO1. LEO1 is a component of the PAF1 complex, which plays numerous
425   roles in transcriptional regulation. The basal transcription factors SNAP50, TFIIS-like protein
426   (LmxM.32.2810), and a hypothetical protein (LmxM.22.0500) with remote homology to TFIIS
427   helical bundle, ISW1 transcriptional elongator (LmxM.22.0500) were identified.   Five
428   components of the cleavage and polyadenylation specificity complex (CPFS) were identified
429   and validated by reciprocal co-IP, as this process occurs co-transcriptionally it must be near
430   polymerase complexes. Additionally, proteins associated with the splicing machinery of
431   *Leishmania* were identified, including LmxM.23.065, a component of the spliceosome. Cap
432   binding proteins and members of the nuclear exosome were also identified, all indicative of
433   the mRNA processing and quality control events that occur alongside transcription of the pre-
434   mRNA. These hits are consistent with the ChIP-seq dataset and show BDF5 is located in sites
435   of polymerase II transcriptional activity.

436

437   The ChIP-seq distribution of BDF5 identified it to be enriched not only at TSS regions but also
438   at rRNA and tRNA genes and some polymerase II termination sites (cSSRs). It was interesting
439   to discover proteins in the XL-BioID that are involved in the maturation of both tRNAs and
440   rRNAs, placing BDF5 in proximity to the transcription and maturation of different classes of
441   RNAs. Base J is associated with termination sites in *Leishmania*[59]*, and the base J-associated
442   glucosyltransferase JBP1 (LmxM.36.2370) was found to be 3-fold enriched over the control,
443   potentially indicating that BDF5 may occasionally be found at sites linked to transcriptional
444   termination. Interestingly, many factors associated with the detection and repair of DNA
445   damage were also found in the proximal proteome, together with factors associated with
446   DNA replication. It is known that DNA damage can occur in transcriptionally active regions
447   due to the formation of RNA-DNA hybrids called R-loops[60]. Some of the origins of DNA
448   replication in *Leishmania* coincide with transcriptional start sites, suggesting we can detect
449   this association in the XL-BioID data[61].

450

451   Because the samples were trypsin digested, it was difficult to obtain much information on
452   histone tails. Nevertheless, we were able to detect some peptides from the core of histones
453   and histone variants as significantly enriched in proximity to BDF5. Peptides were detected
454   for H2A.Z, H2B.V, H3 and H3.V. In *T. brucei,* the H2A.Z and H2B.V variants have been localised
455   to divergent SSRs[19], where H2A.Z plays a role in the correct positioning of transcription

456 initiation. H2A.Z and H2B.V are also essential for *Leishmania*[62]. H3.V localises to convergent
457 SSRs in *T. brucei* and is not essential for *Leishmania,* nor does it play a role in transcriptional
458 termination in this organism[62]. Mining the XL-BioID data further we were able to detect a
459 number of acetylated peptides. Acetylation sites were detected on HAT2, BDF8, FHA-like
460 protein (LmxM.35.2500), a putative Rttp106-like histone chaperone and several hypothetical
461 proteins (**Table S2**). However, we were again unable to detect any acetylated peptides
462 derived from histones.

463

464 The capacity of XL-BioID to enrich large amounts of proximal material allows it to be combined
465 with other methods, such as phosphoproteomics[51]. We engineered a cell line to carry
466 BDF5::miniTurboID for faster labelling kinetics and higher temporal resolution, allowing us to
467 explore BDF5-proximal phosphorylation events across the cell cycle of hydroxyurea
468 synchronised cultures. Following synchronisation release, 30 minute biotinylation timepoints
469 were carried out 0 , 4 and 8 h corresponding to G1/S, S and G2/M phase respectively..
470 Samples were processed using the XL-BioID workflow, then proximal phosphopeptides were
471 enriched using Ti-IMAC resin prior to LC-MS/MS analysis. The resulting dataset was compared
472 to a reference phosphopeptide dataset derived from the kinetochore protein KKT3[51]. Two
473 BDF5-proximal phosphopeptides were identified in early-S phase which then rose to 19 and
474 13 as the cells progressed through the S and G2/M phases respectively (**Fig. S9, Table S3**). Of
475 these, 14 unambiguous phosphosites were detected in total for proteins in proximity to BDF5,
476 including several for BDF5 itself, pS135, pS133, pS317 and pS330. S135 and S133 are located
477 between the two bromodomains, while S317 and S330 are located after the second
478 bromodomain. LmxM.35.2500, which was highly enriched in the original XL-BioID and
479 identified to contain a putative FHA domain, was itself found phosphorylated at S202, S208
480 and S545. LmxM.33.2300 (BDF8) was found to contain an ambiguous phosphosite at one of
481 six sites in the region of S50-S61 (**Fig. S9**). Despite detecting multiple phosphosites, only a
482 single protein kinase was identified in proximity to BDF5, LmxM.25.1520 (LBPK3), an orphan
483 kinase with unknown function that has been reported to bind lapatinib[63].

484

485 The combined ChIP-Seq and XL-BioID data defined where BDF5 localises on the genome, and
486 the protein landscape around it. This points towards a role for BDF5 in promoting
487 transcriptional activity and provides a starting point to develop assays to characterise the
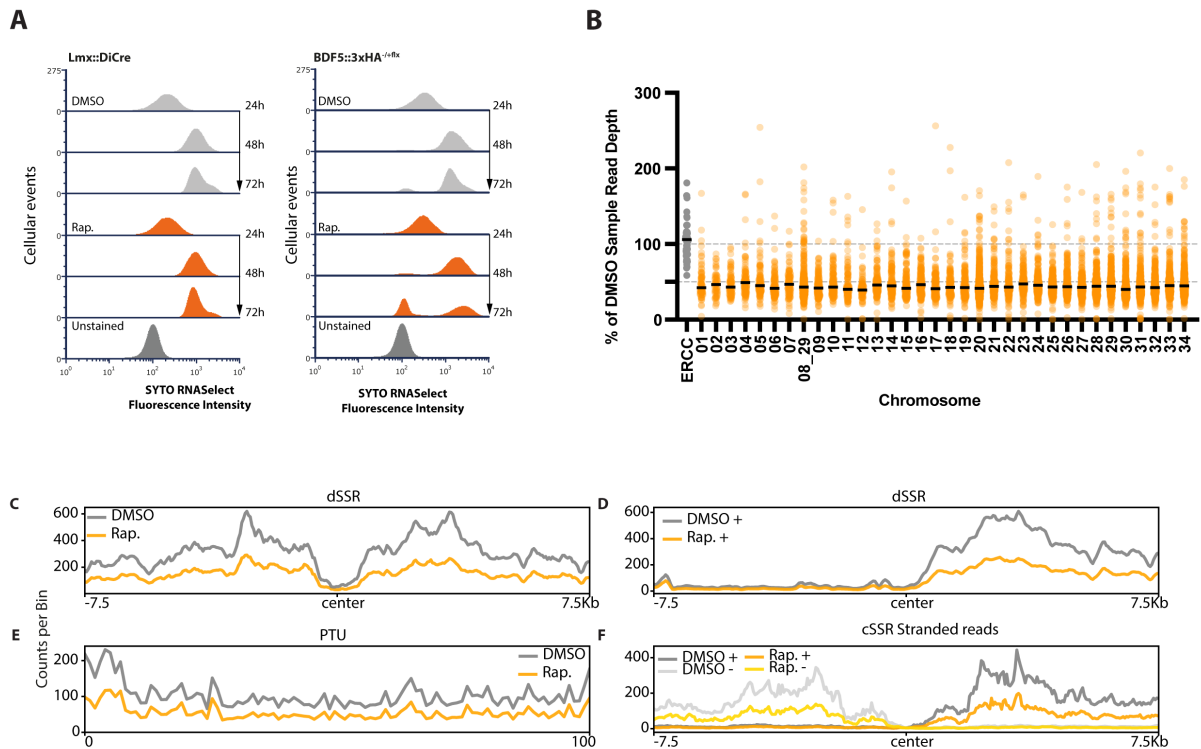488 phenotypes of BDF5-induced null strains.

489

490

491

492

BDF5 depletion results in generalised transcriptional defect.

Figure 6: Effect of BDF5 depletion on RNA levels and gene expression. A. Flow cytometry of cells stained with SYTO RNASelect Stain to measure total RNA levels in *Lmx DiCre* strains or the *BDF5⁻/⁺flx* strain treated with rapamycin or DMSO over a 72 h time course. 20,000 events measured per condition. **B**. Dot plot of total RNA-seq reads per protein-coding gene scaled to ERCC spike-in controls, then as a percentage of the DMSO control sample, separated per chromosome, conducted at a 96 h timepoint. Black lines denote the median. N=3 **C**. Metaplot divergent SSR (n=60) for DMSO treated or rapamycin-treated *BDF5⁻/⁺flx*. **D**. Metaplot of reads mapping to the + strand, normalised to ERCC control at divergent SSRs (n=60) of DMSO treated or rapamycin-treated *BDF5⁻/⁺flx* cultures. **E**. Metaplot of + stranded RNA-seq reads normalised to ERCC spike-in controls for PTUs (n=120), on a scale of 0-100%. **F**. Metaplot of reads mapping to the + and − strands, normalised to ERCC control at convergent SSRs (n=40) of DMSO treated or rapamycin-treated *BDF5⁻/⁺flx* cultures. Metaplot data is from 1 representative of the three replicate RNA-seq datasets.

As most of the BDF5 enriched regions of the genome corresponded to transcriptional start sites, and the proximal proteome contained factors associated with the transcription and maturation of various classes of RNA we sought to assess the effect of BDF5 depletion on cellular RNA levels. Promastigote cultures were stained for total RNA content using SYTO RNASelect fluorescent stain at 24, 48 and 72 h timepoints and measured by flow cytometry (**Fig. 6A**). For *Lmx::DiCre* strain, the addition of rapamycin caused no changes in the levels of total RNA staining. SYTO RNASelect staining increased as cells progressed through log phases of growth at 48-72 h time points. However, once BDF5 was deleted from the *BDF5::6xHA⁻/⁺flx*

519   cell line by the addition of rapamycin, there was a pronounced increase in the number of
520   cellular events containing very low levels of RNA staining, such that the profile at 72 h overlaps
521   with that for with unstained control cells. This result suggested that total levels of
522   transcription were reduced upon BDF5 deletion from cells. We investigated this in more detail
523   by using total, stranded RNAseq that included External RNA Controls Consortium (ERCC)
524   Spike-in controls[20]. Cultures of *BDF5::6xHA$^{-/+flx}$* treated with Rapamycin or DMSO were
525   harvested, then RNA extraction buffer spiked with the 92 synthetic ERCC RNAs was used to
526   lyse the parasites for RNA purification. Following sequencing and read mapping these RNAs
527   were then used to provide a normalisation channel. Overall, a >50% reduction in the median
528   read depth was observed across protein-coding genes on all chromosomes (**Fig. 6B**). When
529   normalised read depths were compared using metaplots of divergent SSRs, this ~50%
530   reduction in transcriptional levels was reflected (**Fig. 6C**). However, no positional effects were
531   observed on transcriptional start sites (**Fig. 6D**). The 50% reduction in read depth was
532   reflected across PTUs (**Fig. 6E**) and at convergent SSRs (**Fig. 6F**). Strand-specific read depth at
533   cSSRs did not indicate any increase in transcriptional readthrough in BDF5-induced null cells
534   (**Fig. 6F**), suggesting the BDF5 located at these termination sites is not playing a role in
535   transcriptional termination. Overall, these results indicate BDF5 is important for global pol II-
536   dependent gene transcription.

537

538   Transcriptionally active regions of kinetoplastid genomes often accumulate DNA damage
539   which occurs due to the formation of DNA-RNA hybrids (R-loops)[60,64]. As we detected proteins
540   involved in co-ordinating DNA repair in the BDF5 proximal proteome, and that this appears
541   to be a broader feature of BDF protein networks[65,66], we examined if there was a link between
542   BDF5 and the DNA damage response in *Leishmania*. *BDF5*-induced-null promastigotes cease
543   growing quickly, whereas parasites deficient for genome-stability factors often die slowly[50],
544   suggesting maintaining genome integrity is not the primary role of BDF5. Indeed, after using
545   western blotting to detect γH2A phosphorylation[67], a sensitive marker for the cellular
546   response to DNA damage, we could not detect any increase in γH2A signal in BDF5-depleted
547   cells, nor was there any detectable difference in the γH2A response of these cells to a non-
548   specific DNA damaging agent, phleomycin (**Fig. S10**). This indicates that there is no direct or
549   secondary role for BDF5 in DNA damage response. Despite enrichment in the BDF5 proximal
550   proteome for mRNA splicing factors, we did not find evidence to support trans- or cis-splicing
551   defects in BDF5 induced-null mutants using a qualitative RT-PCR assay. This assay was capable
552   of detecting splicing defects caused by inhibition of an analog-sensitised CRK9 by the bulky
553   kinase inhibitor 1NM-PP1(**Fig. S11, S12**)[68].

554

555   **Discussion**
556   Kinetoplastid parasites have evolved a genomic architecture that requires them to conduct
557   most gene transcription constitutively, in an apparently simplified manner and deal with
558   consequences of this using post-transcriptional regulation and specialised solutions to genes
559   requiring a "high-dose"[8]. Pol II transcriptional start sites may simply be maintained as open

560   chromatin. However, recent evidence has indicated these regions are actively regulated,

561   particularly through histone acetylation. How the cell interprets these marks is not completely

562   understood. Bromodomains are clearly critical components of this process in *Leishmania*; we

563   were unable to generate null mutants in five of the seven bromodomain encoding genes, also

564   implying there is no redundancy in their individual functions. Although failure to generate a

565   null is the most basic standard of genetic evidence for essential genes[44], we were able to

566   generate high-quality, genetic target validation for BDF5, using inducible DiCre both in the

567   promastigote stage and during murine infections. BDF5 expression was confirmed in both

568   stages and expression levels were correlated with cellular growth rate in promastigote stages.

569   Combined with the rapid cytostatic phenotype occurring upon BDF5 inducible deletion,

570   followed by cell death, this identifies BDF5 as a regulator of cell growth and survival. This

571   finding demonstrates that the interpretation of histone acetylation is important for cellular

572   survival (**Fig. 7**), although for *Leishmania* the specific histone PTMs found at TSSs are not

573   currently defined.

574

575   When functionally characterising BDF5, our starting hypothesis was that BDF5 would localise

576   to polymerase II transcriptional start sites, so it was surprising to find BDF5-enriched peaks

577   associating with many other sites such as rRNA genes, tRNA genes and convergent strand

578   switch regions. This suggests BDF5 plays a multipurpose or generalist role in recruiting or

579   regulating chromatin to promote transcription by multiple polymerase complexes. This was

580   further emphasised by the proximity proteomics dataset, which revealed BDF5 to be close to

581   proteins involved in different processes linked to transcriptionally active chromatin, in

582   particular RNA maturation factors, DNA repair factors and polymerase associated complexes.

583   Our phenotypic analysis appeared to rule out roles for BDF5 in influencing the DNA damage

584   response and cis- and trans-splicing of mRNA but did demonstrate that it was required for

585   normal transcription of polymerase II PTUs. Due to the rRNA depletion method used and low

586   coverage over tRNA genes, we could not assess if pol I or pol III transcripts levels were

587   reduced. This could be determined using qPCR in future studies. Spike-in controlled total RNA

588   seq was previously used to study the influence of HAT1 and HAT2 on transcription in *T. brucei*

589   [20]. It is striking that BDF5 knockout in *L. mexicana* phenocopies HAT1 knockdown in *T. brucei*,

590   both resulting in an overall reduction in transcription levels. In *T. brucei,* HAT1 is required for

591   acetylation of H2A.Z and H2B.V. Depletion of HAT1, and thus H2A.Z levels, leads to a 10-fold

592   decrease in the amount of chromatin-bound pol II, resulting in 50% reduced transcriptional

593   activity. Intriguingly, pol II levels at TSSs were not affected by this; the authors suggested

594   H2A.Z acetylation is required for optimal transcription of bound pol II. As BDF5 knockout

595   phenocopies HAT1 depletion and results in lower pol II activity, it might therefore be involved

596   in reading or applying acetylation of H2A.Z. Surprisingly, although we find HAT2 proximal to

597   BDF5, HAT1 was neither enriched nor detected in our XL-BioID dataset. This suggests that

598   there is a distinct spatial separation between BDF5, HAT2 and HAT1 in *Leishmania* (assuming

599   there is no technical reason HAT1 cannot be labelled by XL-BioID). BDF5 also did not co-

600   precipitate very strongly with HAT2 (**Fig. S8**), suggesting any interaction between them might

601   be transient or indirect. We did not observe changes in the positioning of transcription
602   initiation, suggesting the HAT1/BDF5 phenotype over-rides any effect on HAT2 dysfunction if
603   this is indeed a BDF5 complex member. Purified *L. donovani* HAT2 has been shown to
604   acetylate H4K10 and it appears to be essential as only heterozygotes can be generated using
605   traditional knockout strategies[15,18,69]. *L. donovani HAT2*^{-/+} heterozygotes grow slowly and
606   display a cell-cycle defect. No effect was determined on transcriptional initiation positioning
607   at TSSs but an S-phase cell cycle-dependent reduction on *CYC4* and *CYC9* genes was
608   reported[18]. Future work could investigate the requirement of BDF5 for cell cycle dependent
609   gene transcription in *Leishmania*, which is an interesting observation given the lack of obvious
610   gene specific promoters.

611

612   A recent immunoprecipitation dataset of *T. brucei* chromatin factors[22] defined a complex
613   consisting of BDF5, BDF3, HAT2 and orthologs of the hypothetical genes LmxM.24.0530,
614   LmxM.22.0880, LmxM.35.2500, LmxM.33.2300, LmxM.08_29.1550 that were highly enriched
615   in our proximity proteome (**Fig. 4**). We propose that these proteins represent a Conserved
616   Kinetoplastid Regulator of Transcription (CRKT) Complex, that is recruited to acetylated
617   histones at TSSs (**Fig. 7**). The association of BDF5 at transcriptional termination regions, albeit
618   in lower amounts, could indicate that BDF5 is included in a mobile complex that can progress
619   along chromatin and accumulates at start and termination sites. One complex could be the
620   PAF1 complex, a multifunctional complex associated with pol II initiation, elongation, pausing
621   and termination[70]. However, PAF1-complex is poorly characterised in kinetoplastids and the
622   PAF1 protein itself lacks identifiable orthologs in these organisms. *T. brucei* BDF5 has been
623   suggested as a potential component of a transcription initiation complex due to its dual
624   bromodomains and the interaction with proteins containing homology to TFIID TAF1 (which
625   also contains 2 bromodomains as well as protein kinase and acetyltransferase function).

626

627   Our findings further illustrate the strength of proteomic approaches to studying chromatin
628   regulation in kinetoplastids where the large TSSs allow plentiful material to be derived[20].
629   Combined with XL-BioID this allowed for the enrichment of PTMs to be determined for many
630   of the complex members. The phosphorylation of the region connecting the two BDs might
631   represent a site of PTM-dependent regulation of BDF5. Regulation of BDF function by
632   phosphorylation has been reported, for example, BRD4 is phosphorylated in mitosis and
633   hyperphosphorylated BRD4 is associated with greater transcriptional activity during
634   oncogenesis[71,72]. Adaptation of the XL-BioID workflow to include a chemical derivatisation
635   step (e.g. stable isotope acylation) could allow it to be used to detect histone tail peptides in
636   proximity to BDF5 or other BDFs, potentially identifying their native binding partners and
637   providing locus-specific views of histone PTMs.

638

639   As bromodomains are chemically tractable targets it may be possible to develop *Leishmania*
640   specific inhibitors that target BDF5. Such a compound would be of high value to the
641   investigation of BDF-dependent transcriptional regulation in kinetoplastids, allowing for

642 precise temporal disruption of BDF5 and the processes that it coordinates. It should be noted
643 that parasites expressing BDF5 with singly mutated bromodomains were viable, requiring
644 both to be disrupted to observe a reduction in parasite growth. Potential BDF5 inhibitors
645 would likely require a bi-specific molecule, a PROTAC (proteolysis targeting chimera) molecule
646 (not yet realised in kinetoplastids), or a mono-specific inhibitor that can perturb the complex
647 enough to be fatal for the cell.

648

649 In summary, our findings identify the importance of the linkage between histone acetylation
650 and transcriptional regulation by bromodomain factors in a eukaryote that is divergent from
651 opisthokonts such as the humans host. Because of their unusual features, kinetoplastids can
652 provide ideal organisms to investigate the evolution of chromatin regulation by acetylation.

653
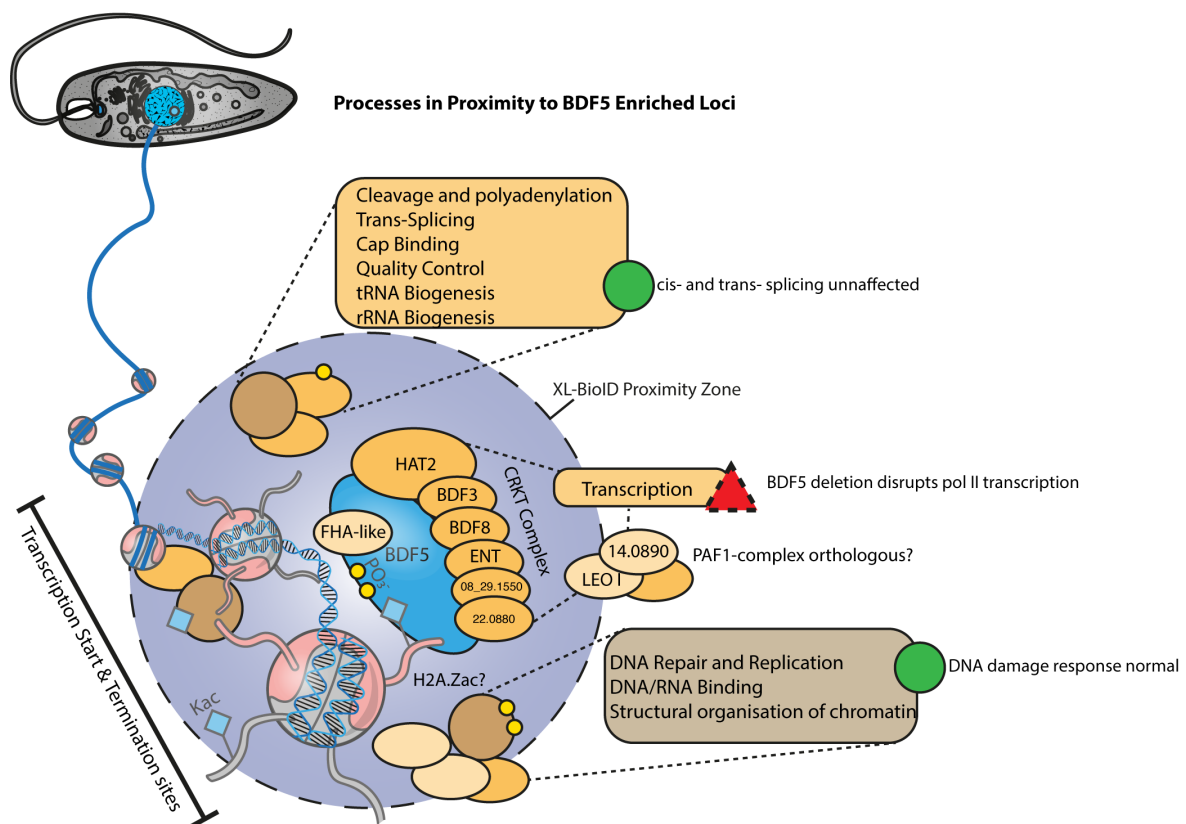
654

655 **Figure 7: Cartoon of the BDF5-defined chromatin landscape.** BDF5 localised to chromatin with
656 the CRKT complex members depicted as interacting directly and influencing transcription.
657 Juxtaposition of complex members is for illustration only. Not to scale.

658

659 **Acknowledgements**

672   **Author Contributions**
673   NGJ, FC, AJW and JCM conceived the project. JCM, AJW, RG, JM and FC supervised the
674   project. NGJ and JCM designed the experiments. NGJ, VG, GM and JBTC performed the
675   experiments. NGJ, VG, GM and KN analysed experimental data. NGJ wrote the manuscript
676   and all other authors revised it. NGJ, RP, IR, FC, AJW and JCM acquired funding.
677

678   **Data Availability**
679   Mass spectrometry data sets and proteomic identifications are available to download from
680   MassIVE (MSV000087750), [doi:10.25345/C5G543] and ProteomeXchange (PXD027080).
681   ChIP-Seq and RNA-Seq reads are available as FASTQ files at the European Nucleotide Archive
682   under the accession code PRJEB46800.
683

684   **Supplemental Files**
685
686   Table S1: Excel spreadsheet, List of Oligonucleotides, plasmids, cell lines and antibodies
687   used in this study.
688
689   Table S2: Excel spreadsheet, SAINTq Analysis of BDF5 XL-BioID data to identify proximal
690   proteins, also contains list of remote homology identified in hypothetical proteins by
691   HHPRED analysis.
692
693   Table S3: Excel spreadsheet, BDF5 proximal phosphosites through the cell cycle as
694   determined by limma analysis of phosphoproteomic XL-BioID samples.
695

Methods

Molecular Biology

Computational sequence analysis, design of vectors, primers and PCR fragments was performed using CLC Main Workbench (Qiagen). Oligonucleotides were synthesised by Eurofins Genomics. High-fidelity PCRs were conducted using Q5 DNA polymerase (NEB) according to manufacturer's instructions. Low-fidelity screening PCRs were conducted using Ultra Mix Red (PCR Biosystems) according to manufacturer's instructions. Vectors for DiCre strain generation were generated as previously described[45] using Gateway Assembly (Thermo Fisher). PCR amplicons were resolved in 1% agarose (Melford) TBE gels containing 1x SYBRsafe and visualised on a Chemidoc MP (BioRad). A full list of oligonucleotides and vectors are presented in **Table S1**. Sanger sequencing to verify plasmids etc. was conducted by Eurofins Genomics.

Protein samples of cells were generated by taking 2.5×10^7 log phase promastigotes, lysing in 40 µl LDS (lithium dodecyl sulfate) sample buffer supplemented to 250 mM DTT and heated to 60 °C for 10 minutes, after cooling, 1 µl of Basemuncher (Abcam) was added and the sample incubated at 37 °C to degrade DNA and RNA. Samples were separated in TGX Stain-Free SDS-PAGE Gels (BioRad) and the total protein labelled and visualised using a proprietry trihalo compound activated by UV light in a BioRad ChemiDoc MP. Western blotting was performed using an iBlot II (Invitrogen) and the associated PVDF cassettes, using program P0. Membranes were blocked with 5% milk protein in 1x Tris Buffered Saline Tween-20 0.05%. Primary and secondary antibodies are listed in **Table S1** and were detected using appropriate fluorescent channels of chemiluminescent channels of a Chemidoc MP (BioRad), using Clarity Max Western ECL Substrate (BioRad).

Parasites

Leishmania mexicana (MNYC/BZ/62/M379) derived strains were grown at 25°C in HOMEM (Gibco) supplemented with 10% (v/v) heat-inactivated foetal calf serum (HIFCS) (Gibco) and 1% (v/v) Penicillin/Streptomycin solution (Sigma-Aldrich). Where required parasites were grown with selective antibiotics at the following concentrations: G418 (Neomycin) at 50 µgml^{-1}; Hygromycin at 50 µg ml^{-1}; Blasticidin S at 10 µg ml^{-1}; Puromycin at 30 µg ml^{-1} (antibiotics from InvivoGen).

CRISPR/Cas9

Initial screening for bromodomain gene essentiality was performed with a modification of the approach developed by the Gluenz lab[42]. Per gene a single sgRNA was designed with EuPaGDT[73] to target the interior of the coding DNA sequence. Oligonucleotides are defined in **Table S1**. Thirty residue homology flanks were identified adjacent to the CDS and appended to oligonucleotides designed to amplify drug resistance markers from blasticidin and neomycin drug resistance plasmids pGL2208 and pGL2663 respectively. After amplification of the sgRNA

737   and resistance marker the PCR mixes were pooled and precipitated using standard ethanol

738   precipitation, resuspended in sterile water and added to a transfection mix with 1×10^7 mid-

739   log promastigotes. The cell line used was *L. mexicana T7/Cas9::HYG::SAT* [42]. Transfection was

740   performed with an Amaxa Nucleofector 4D using program FI-115 and the Unstimulated

741   Human T-Cell Kit. The mix was resuspended in 10 ml HOMEM 20% FCS and immediately split

742   in two 5 ml aliquots. Following 6-18 h of recovery time the parasites were plated at 1:5, 1:50

743   and 1:500 dilutions in media containing the selective drug blasticidin or G418. Endogenous

744   tagging was performed using the pPLOT 3xMYC::mNG BSD donor vector to install N-terminal

745   tags to BDF5, preserving the 3' UTR for native mRNA regulation (Oligonucleotides defined in

746   **Table S1**).

747

748   *DiCre*

749   DiCre strains for BDF5 were generated as previously described[46]. Briefly the BDF5 CDS and

750   flanking regions were assembled into floxing or knockout plasmids using Gateway cloning,

751   BDF5 was cloned into pGL2314 to fuse a 6xHA C-terminal tag and flank with loxP sites

752   (**Oligonucleotides defined in Table S1**). The BDF5::6xHA^{flx} was first integrated into parasites

753   with clones being assessed for correct integration, correct genome copy number and

754   inducibility of the excision of BDF5^{flx} gene prior to the second round of transfections to delete

755   the remaining wild-type allele. The same quality controls were performed when selecting final

756   clones with the genotype *Leishmania mexicana DiCre::Puro Δbdf5::HYG*

757   *::BDF5::6xHA::flx::BSD.*

758

759   Inducible deletion of BDF5^{flx} in DiCre cell lines was initiated by the addition of 300 nM

760   rapamycin (Abcam) to promastigotes cultures at 2×10^5 cells ml^{-1}. Cells were grown for 48 h

761   then passaged into new media at a concentration of 2×10^5 cells ml^{-1}; induction was

762   maintained by the addition of 100 nM of rapamycin to suppress escape mutants.

763

764   *Clonogenic assays*

765   For clonogenic assays, mid-log cells were counted and then diluted to 1 cell per 800 μl and

766   plated out into 200 μl volumes in 3 x 96-well plates to yield approximately 100 clones. Cells

767   were plated in media ± 100 nM rapamycin and incubated at 25°C for 3 w before counting of

768   viable colonies by both visual screening and microscopic analysis

769

770

771   *Addback strains*

772   To generate episomal addbacks the BDF5 CDS was amplified from *L. mexicana* genomic DNA

773   and cloned into the pNUS C-Ter GFP NEO (pGL1132) using HiFi Assembly (NEB) to generate a

774   complementation vector. This was used as a base for site-directed mutagenesis using the Q5

775   Mutagenesis product (NEB) to generate mutations in the conserved asparagine residues N90

776   (OL9577 and OL10352), N257 (OL9579 and OL10353) to phenylalanine in BDF5 BD5.1 and

777   BD5.2 (**Table S1**). Log-phase promastigotes were transfected with 2-5 µg plasmid DNA as

778   previously described and maintained as population under G418 selection.

779

780   *Inducible overexpression*

781   An adaptation of a published method was performed whereby BDF5::GFP alleles generated

782   for episomal addback were amplified using PCR primers OL11307 and OL11308, where the

783   oligonucleotide included a directional loxP site as well as a homology region for HiFi Assembly

784   into pRIB Neo (pGL1132). The vector backbone was linearised with PacI/PmeI double digest,

785   separated by agarose gel electrophoresis and purified using QiaEx II gel extraction resin

786   (Qiagen). Log-phase promastigotes were transfected with 1-5 µg and cloned by limiting

787   dilution. Clones were induced to express BDF5::GFP or BDF5$^{NN>FF}$::GFP

788

789   *Mouse infections*

790   All experiments were conducted according to the Animals (Scientific Procedures) Act of 1986,

791   United Kingdom, and had approval from the University of York Animal Welfare and Ethical

792   Review Body (AWERB) committee. All animal studies were ethically reviewed and carried out

793   in accordance with Animals (Scientific Procedures) Act 1986 and the GSK Policy on the Care,

794   Welfare and Treatment of Animals. Mid-log parasites were treated with 500 nM rapamycin

795   and allowed to progress to stationary phase. These cultures were used to infect BALB/C mice

796   at a dose of 2 x 10^5 parasites per footpad. Infections were allowed to progress for 8 w, at

797   which point mice were euthanised and footpads and popliteal lymph-nodes were dissected

798   for mechanical disruption and determination of parasite burden by limiting dilution, as

799   previously described[74].

800

801   *Live-Cell Microscopy*

802   To image mNeonGreen::BDF5 10^6 mid-log cells were incubated with 1 µg ml^{-1}Hoechst 3342

803   for 20 mins at 25°C to stain DNA, harvested by centrifugation at 1200 x g for 10 mins and

804   washed twice with PBS. Cell pellets were resuspended in 40 µl CyGel (BioStatus) and 10 µl

805   settled onto SuperFrost+ Slides (Thermo) then cover slip applied. Cells were imaged using a

806   Zeiss AxioObserver Inverted Microscope equipped with Colibri 7 narrow-band LED system and

807   white LED for epifluorescent and white light imaging. Cells were imaged using the x63 or x100

808   oil immersion DIC II Plan Apochromat objectives. Hoechst signal was imaged using the 385

809   nm LED and filter set 49, mNeonGreen with the 469 nm LED and filter set 38. Z-stacks were

810   obtained using the Zen Blue software to control the system and exported as .CZI files to be

811   processed in ImageJ using the Microvolution blind deconvolution module. Wavelength

812   parameters were set for Hoechst (497 nm) and mNeonGreen (517 nm) emission and

813   refractive index parameters were defined for Cygel (1.37). Blind deconvolution was iterated

814   100 times using the scalar setting. Maximum intensity projections were then exported as

815   were individual Z-planes for subpanels in TIFF format. Amastigotes in murine bone marrow

816   derived macrophages were grown on glass bottomed 35 mm dishes (Thermo Scientific) and

817   imaged in FluoroBrite DMEM (Gibco) using a heated plate holder to maintain the samples at

818   35°C. In this instance due to the short imaging duration CO_2 supplementation was not
819   provided.

820   *XL-BioID*

821   BDF5 and KKT19 were N-terminally tagged with BirA* [42] and then cultures were grown to mid-
822   log phase. For the final 18h of growth biotin was added to the medium at 150 µM, 4 x 10^8
823   parasites were washed twice in PBS and limiting cross-linking was performed with 1 mM
824   dithiobis(succinimidyl propionate) (DSP) for 10mins at 26 °C in PBS. After quenching with
825   20mM Tris pH 7.5 for 5mins, cell pellets were washed in PBS and then lysed in RIPA buffer
826   supplemented with protease inhibitors followed by Benzonase treatment and sonication.
827   Biotinylated and cross-linked proteins were purified using Streptavidin magnetic beads
828   (MagResyn) which were washed with a series of harsh washes before cross-linker reversion
829   and on bead digest with Trypsin Lys-C (Promega). Peptides were then desalted and prepared
830   for mass spectrometry. For a full protocol see *Geoghegan et al.* [51]

831

832   Hypothetical proteins were screened for remote structural homology using HHPRED [31] and
833   Phyre2 [75] to identify putative domains in these proteins.

834

835   *Co-Immunoprecipitation*

836   Co-immunoprecipitation to confirm BioID hits was performed by tagging candidate proteins
837   with 3xHA::mCherry PURO using an adapted pPLOT vector (gifted by Ewan Parry, Walrad Lab.)
838   in the *L. mexicana* T7/Cas9 3xMYC::mNG::BDF5 strain previously generated. Correct
839   integration of the tag was confirmed by western blotting for the HA epitope. For pulldowns,
840   30 ml of mid-log cultures (~1.5 x 10^8 cells) were harvested, by centrifugation at 1200 x g for
841   10 minutes and resuspended in PBS. DSP reversible cross-linker (dithiobis(succinimidyl
842   propionate) (Thermo) was added to 1 mM and incubated for 10 mins at 26 °C. Cross-linking
843   was quenched by the addition of Tris pH7.5 to 20 mM and parasites washed with PBS. The
844   cells were then lysed using 1x RIPA buffer (Thermo) supplemented with 3x HALT Protease
845   inhibitors (Thermo) and 1 x PhosSTOP (Roche), 2 µl (500 Units) BaseMuncher Endonuclease
846   (Abcam). The lysate was sonicated 3 x 10 seconds at 40% amplitude using a probe sonicator
847   (Sonics Vibra-Cell) and then clarified by centrifugation 10, 000 x *g* for 10 mins at 4 °C. HA-
848   tagged bait proteins were then immunoprecipitated by the addition of 30 µl anti-HA magnetic
849   beads (Pierce) incubated for 2 hours with rotation at 4 °C. The beads were then washed 3
850   times using the supplemented RIPA lysis buffer and proteins eluted from the beads using 40
851   µl 1x LDS buffer supplemented with 250 mM DTT and heating to 60°C for 10 mins. The eluted
852   fractions were analysed for presence of the BDF5 prey protein and intended bait proteins by
853   western blotting for the MYC and HA epitopes respectively.

854

855   *ChIP-Seq*

856   BDF5 ChIP-seq was performed using a modification of a protocol previously optimised for *T.*
857   *brucei* [60] and the ChIP-it Express Enzymatic Kit (Active Motif). *Lmx DiCre BDF5::6xHA$^{-/+flx}$*
858   parasites were grown to 5 x 10^6 cells ml^{-1} in sufficient volume to collect 3 x 10^8 cells per ChIP

859 replicate. Cells were fixed with 1% formaldehyde for 5 mins then quenched with 1x of the
860 included glycine solution. Fixed cells were Dounce homogenised until only nuclei were visible
861 by microscopy. Following enzymatic digestion of purified nuclei, the mix was sonicated 3 x 10
862 seconds at 40% amplitude using a probe sonicator (Sonics Vibra-Cell) to increase recovery of
863 mono- to tetra-nucleosomes[54]. Chromatin fractionation and release was checked by agarose
864 gel electrophoresis before immunoprecipitation using anti-HA magnetic beads (Thermo) for
865 2 h at 4 °C. Beads were washed and the cross-linking was reversed following manufacturer's
866 instructions. Liberated DNA and the retained input samples were purified and concentrated
867 using ChIP-cleanup mini-columns (Zymogen). This DNA was quantified using a Qubit (Qiagen)
868 High Sensitivity DNA kit and sent for library preparation. Library generation was performed
869 on a minimum of 5 ng DNA using (TF KIT) in the Genomics Laboratory of University of York
870 Bioscience Technology Facility. Sequencing was conducted at the University of Leeds. Reads
871 were quality checked and trimmed using FastQC version 11.0.5 and Cutadapt version 2.5,
872 respectively. This was followed by alignment to the *L. mexicana* T7/Cas9 genome using BWA-
873 MEM (version 0.7.17). Paired ChIP-seq and input alignment files were normalised to each
874 other using deepTools' bamCompare (version 3.3.1) with SES normalisation and bin size of
875 500. Bigwig files were converted to wig files with UCSC's bigWigToWig tool, and the resulting
876 3 files were combined by taking the mean. Peaks were filtered to only include those with a
877 mean log2 ratio greater than 0.5 and peaks that were less than 5 kb apart were merged.
878 Strand switch regions were defined as regions between the end of a CDS on one strand and
879 the beginning of CDS on the other strand. Data were visualised using IGV (Broad Institute) and
880 Circa software (OMGenomics).
881
882 *Flow cytometry*
883 Flow cytometry of fixed and live cells treated with propidium iodide for cell cycle and
884 live/dead analysis was conducted as previously reported[46]. For determination of total RNA
885 levels by SYTO RNASelect staining, 1 ml of culture was treated with 500 nM SYTO RNASelect
886 for 20 mins at 25 °C. Cells were collected by centrifugation 1200 x *g* for 10 mins and washed
887 with PBS before resuspension in PBS 10 mM EDTA pH 7.4. Cells were analysed using a
888 Beckman Coulter Cyan ADP flow cytometer with detection of the stained RNA in the FL1
889 channel.
890
891 *Stranded ERCC Controlled RNA-seq*
892 Cultures of promastigote *Lmx DiCre BDF5::6xHA$^{-/+flx}$* were treated with DMSO or 300 nM
893 rapamycin for 48 h then passaged to a density of 2 x 10^5 cells ml^{-1} for another 48 h. At this
894 point 2 x 10^7 cells were collected, washed in PBS and processed for total RNA extraction. Total
895 RNA was extracted using Monarch Total RNA Miniprep kit (NEB) as per the manufacturer's
896 instructions with the exception of the addition of ERCC Synthetic RNA Transcripts (Ambion)
897 to the RNA extraction buffer used to lyse the cells. This was added to a final concentration of
898 1/1000 from the manufacturers stock solution. In addition to the on-column Dnase digest, an
899 additional treatment of the eluted RNA was performed with TURBO DNA Free kit as per the

900   manufacturer's protocol. RNA was processed by Novogene using Illumina Ribo Zero method
901   and NEBNext® Ultra™ Directional RNA Library Prep Kit to generate libraries which were
902   sequenced on Illumina NovaSeq 6000 S4 flowcell with PE150. Reads were processed with
903   FASTQC Groomer before mapping with HiSAT. BAM files were converted to bigwig format
904   using bamCoverage (DeepTools) with a scaling factor applied to normalise the total reads to
905   the median ERCC read values. Metaplots were generated using deepTools computematrix
906   and plotProfile tools for dSSR and cSSR in reference-point mode (centre point of the SSR). PTU
907   metaplots were generated using the same tools in scale-regions mode.

908

909   *Splicing RT-PCR*
910   Analog-sensitive CRK9 (LmxM.27.1940) mutants were generated using Cas9 to perform
911   precise genome editing to replace the codon encoding methionine at the gatekeeper position
912   (M501) with a glycine or alanine residue (protocol adapted from[68]). Oligos sequences
913   provided in **Table S1**. The validation of the CRK9 mutants was performed by sequencing using
914   OL11605 and a dose response curve, set at 2.5×10^4 cells ml^{-1} treated with the bulky kinase
915   inhibitors (BKIs: PP1 (1-(1,1-dimethylethyl)-3-(4-methylphenyl)-1H-pyrazolo[3,4-d]pyrimidin-
916   4-amine), 1NM-PP1 (1-(1,1-dimethylethyl)-3-(1-naphthalenylmethyl)-1H-pyrazolo[3,4-
917   d]pyrimidin-4-amine) and 1NA-PP1 (1-(1,1-dimethylethyl)-3-(1-naphthalenyl)-1H-
918   pyrazolo[3,4-d]pyrimidin-4-amine)) in a range concentration varying from 0 to 120 µM. The
919   viability of treated and untreated control was assessed after 72h, using Alamar blue at
920   0.0025% (w/v). The parental T7/Cas9 cell line was used as control for the analog-sensitive
921   CRK9 lines. The inhibition profile was analysed by nonlinear regression using Prism Version 9
922   (GraphPad).

923

924   Cultures of promastigote *Lmx DiCre BDF5::6xHA$^{-/+flx}$* were treated with DMSO or 300 nM
925   rapamycin for 48 h then passaged to a density of 2×10^5 cells ml^{-1} for another 48 h. Positive
926   controls for cis- and trans- splicing defects were provided by treating *L. mexicana T7/Cas9*
927   CRK9^{M501G} with 30 µM 1NM-PP1 for 3 h (15x the EC90 at 72h) . Total RNA was purified using
928   NEB Monarch Total RNA MiniPrep Kit. cDNA was synthesised using NEB ProtoScript II with
929   random hexamers. Triple-primer PCR was conducted to determine the trans-splicing of the SL
930   RNA to LmxM.25.0910 with OL12370, OL12371 and OL12372. cis-splicing of the intron in
931   polyA-polymerase (LmxM.08_29.2600) was detected using OL OL12342 and OL12343. PCRs
932   were performed with PCRBio Ultra Red Mix.

933

934   *Statistics*
935   For routine statistical analyses data were analysed with Prism Version 9 (GraphPad). Western
936   blot quantitation was performed using BioRad Imagelab software using the Stain-Free Total
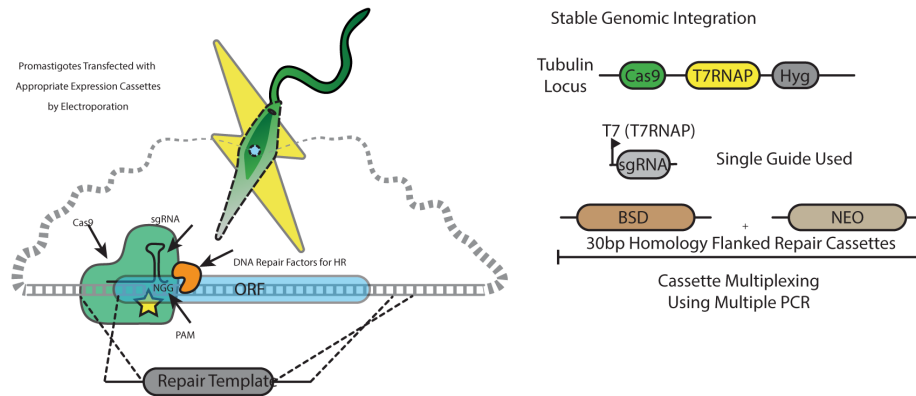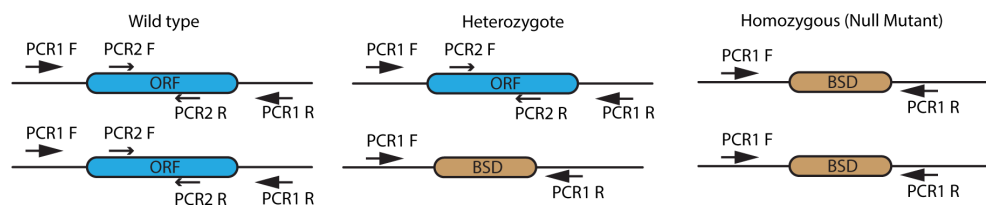937   Protein Channel as the normalisation channel.
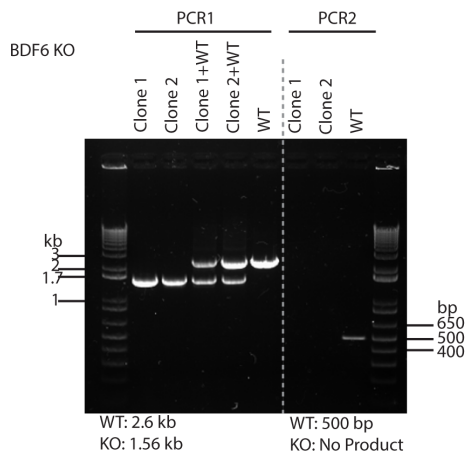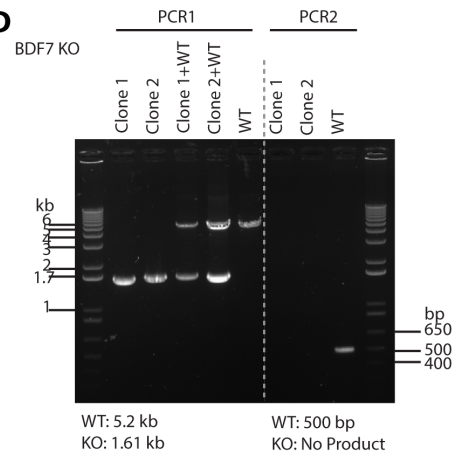
938

939

940

941

942

943   **Supplemental Figures**

944
945
946   **Figure S1: CRISPR/Cas9 screening to identify non-essential bromodomain factors. A**. Cartoon
947   depicting the experimental strategy. **B**. Cartoon depicting the PCR strategy to define gene
948   knockouts isolated from CRISPR/Cas9 screening. **C**. Agarose gel PCR validation of *BDF6* null
949   mutants. **D**. Agarose gel showing PCR validation of *BDF7* null mutants.
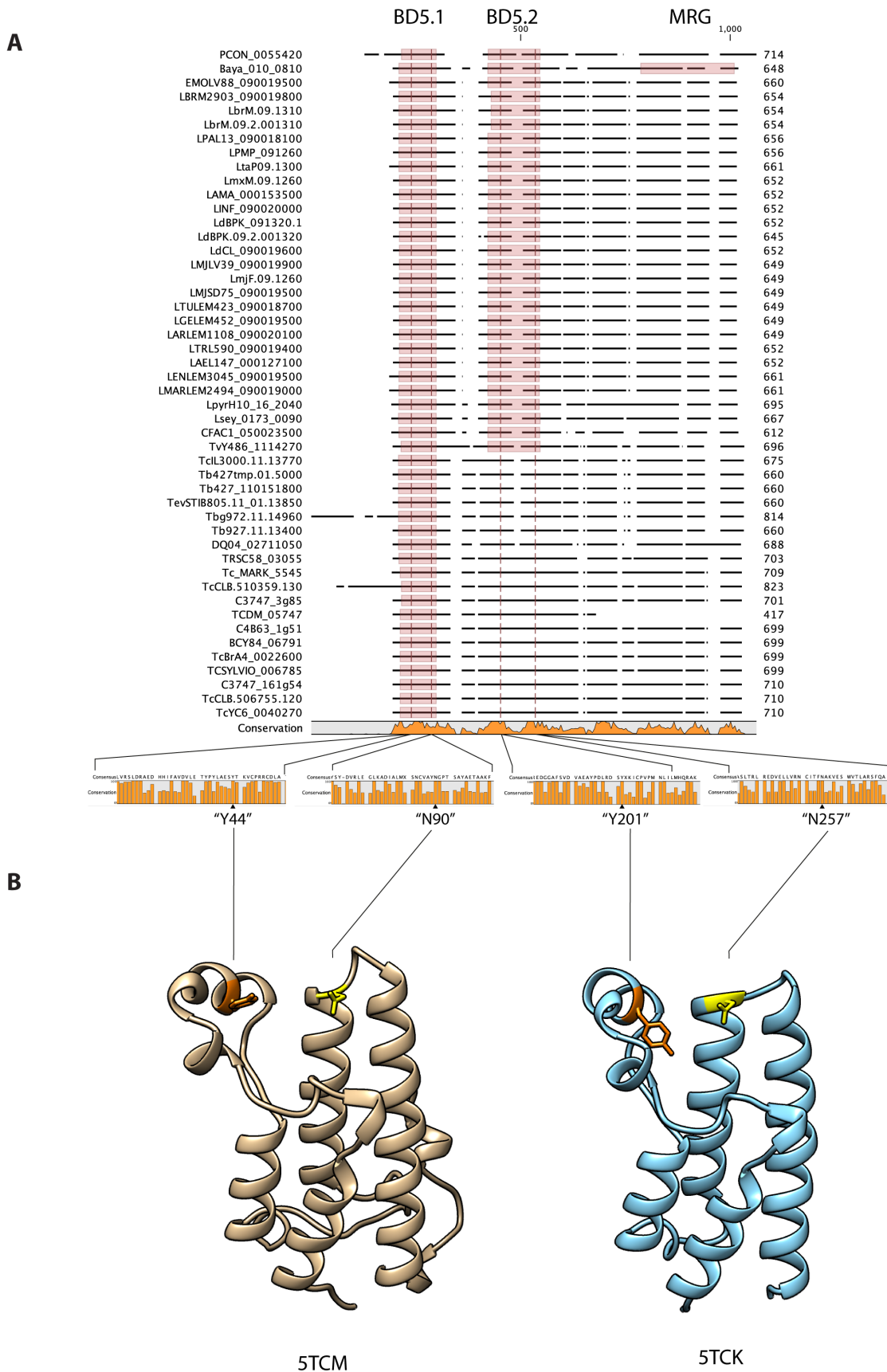
950
Figure S2: CLUSTAL alignment of kinetoplastid BDF5 proteins. A. Amino acid sequences of BDF5
syntenic orthologues were aligned using the Clustal Omega plugin for CLC. Domains that were

953 readily identifiable using the PFAM search plugin are annotated by shaded boxes, conserved
954 tyrosine and asparagine residues are annotated by red lines within the shaded BD5.1 and
955 BD5.2 domains. **B**. X-ray crystal structures of LdBDF5 bromodomains generated by the SGC and
956 deposited at the PDB, conserved tyrosine residues coloured orange and conserved asparagine
957 residues in yellow.
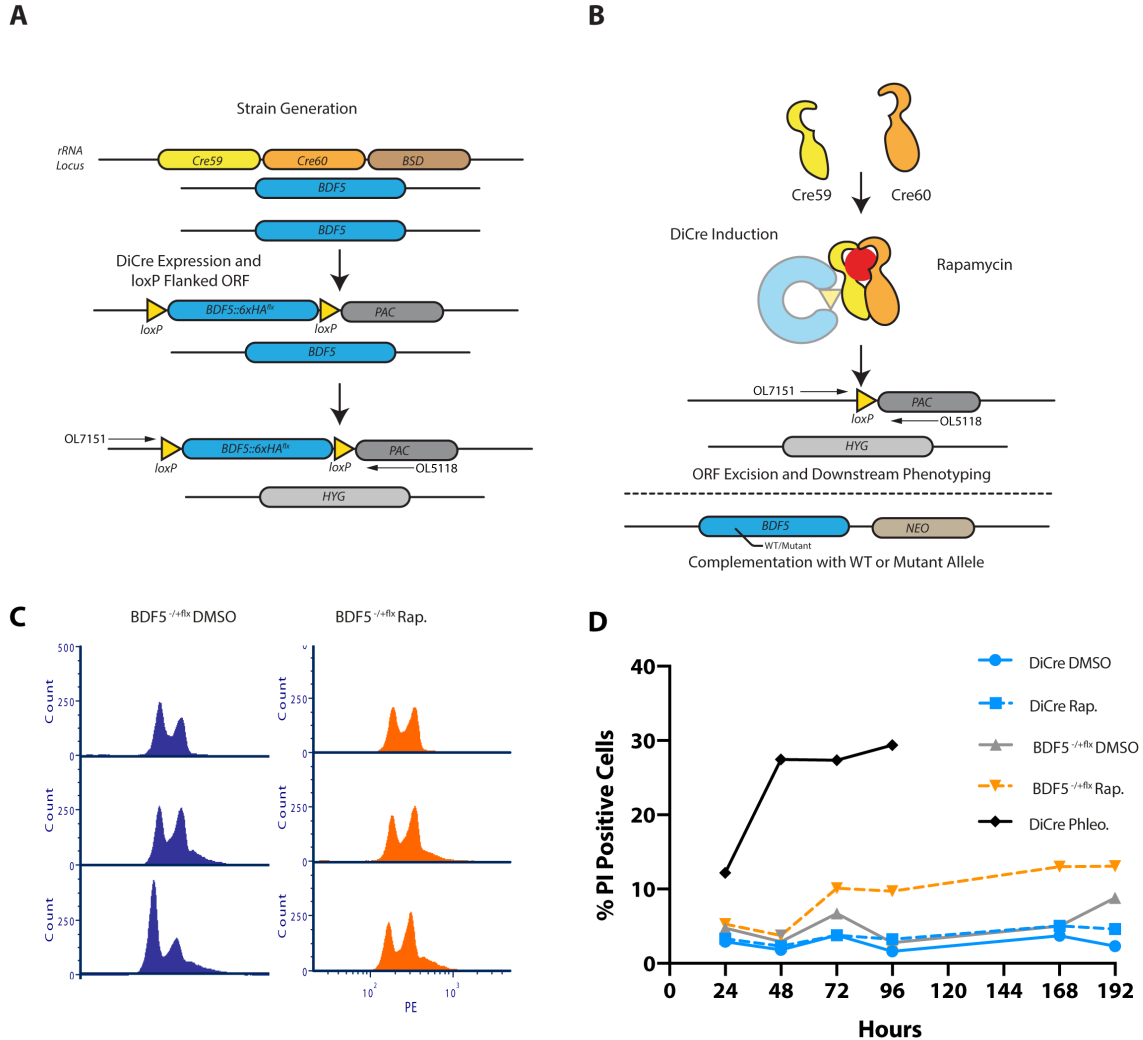
958

959 **Figure S3: Characterisation of BD5 using DiCre Inducible gene deletion in promastigotes.**
960 **A.** Cartoon representation of workflow to generate *Lmx*
961 *::DiCreΔbdf5::HYG/Δbdf5::BDF5::6xHA^{flox}.* **B**. Cartoon representation of floxed allele excision
962 using rapamycin to dimerise the split Cre recombinase, exemplifying the ability to introduce
963 add-back alleles for functional genetics. **C**. Flow cytometry of methanol fixed, RNAse A treated,
964 propidium iodide stained promastigote cultures to characterise the effects of BDF5 knockout
965 on the cell cycle over a 72 h timecourse N=20,000 events. **D**. Live/dead analysis using flow
966 cytometry of non-fixed, propidium iodide treated promastigote cultures following BDF5
967 knockout. A 1 µg/ml phleomycin control was included. Points and error bars indicate mean ±
968 standard deviation, N=20, 000 events.
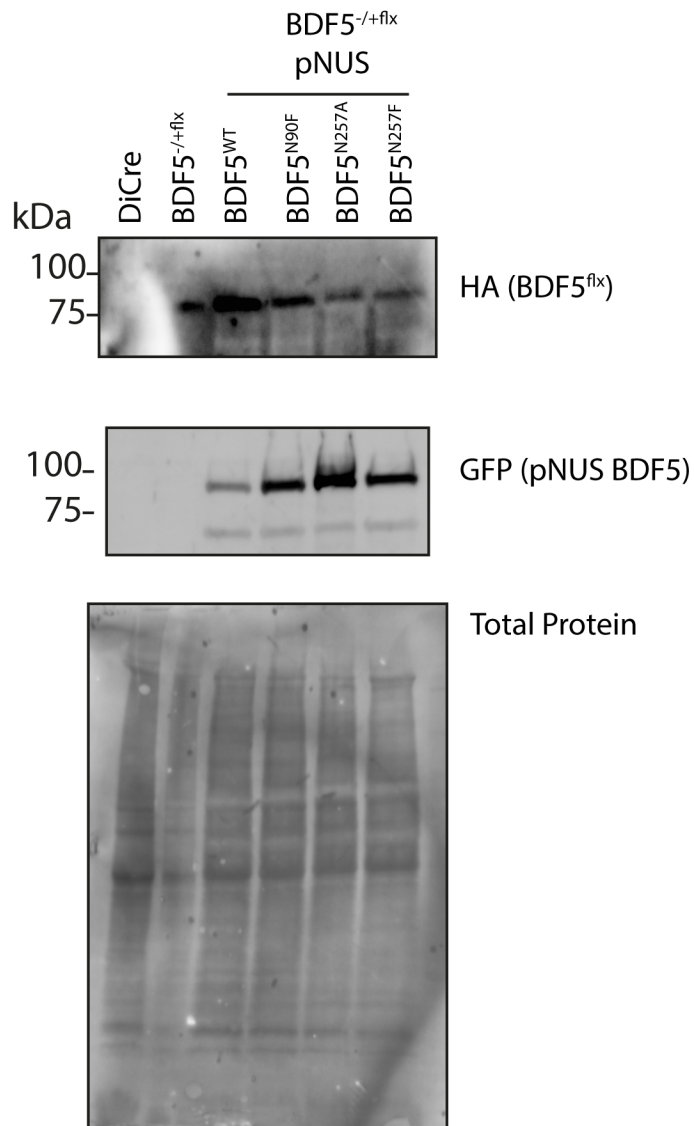
969
970 **Figure S4: Episomal Expression of BDF5 mutant alleles.** Western blot analysis of cell lines
971 expressing BDF5::GFP mutant alleles from pNUS episome vectors in the *Lmx*
972 *::DiCreΔbdf5::HYG/Δbdf5::BDF5::6xHA^flox* background.
973

974
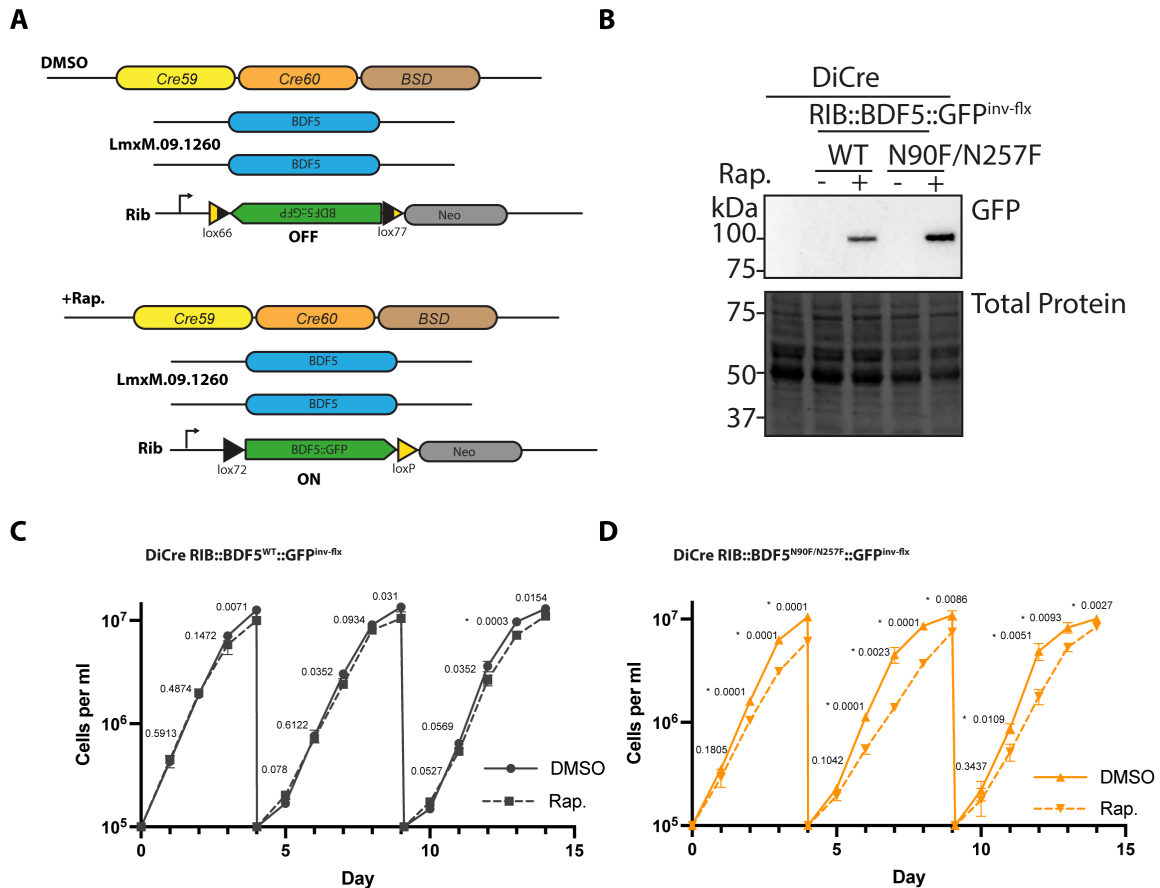
975 **Figure S5: Rapamycin inducible overexpression of BDF5 alleles. A**. Cartoon representing the
976 experimental set-up for expression of an extra BDF5 allele. $BDF5^{N90F/N257F}::GFP$ was cloned into
977 pRIB in an inverted orientation and flanked by directional loxP sites[50] yielding
978 $pRIB::BDF5^{N90F/N257F}::GFP^{inv}$. After integrating this into $Lmx::DiCre,$ clones were isolated and
979 treated with 300 nM rapamycin to induce expression of the BDF5$^{N90F/N257F}$::GFP mutant
980 protein. A control strain was also generated to express a wild-type $BDF5$ allele in the same
981 manner **B**. Western blot analysis of cultures from C and D at the 48 h timepoint of the second
982 growth cycle. **C**. Growth curve of promastigote cultures of $DiCre::BDF5::GFP^{inv-flx}$ treated with
983 rapamycin or DMSO. Data points represent mean values ± standard deviation. N=3 **D**. Growth
984 curve of promastigote cultures of $DiCre::BDF5^{N90F/N257F}::GFP^{in-flxv}$ treated with rapamycin or
985 DMSO. Data points represent mean values ± standard deviation N=3. For C and D repeated t-
986 tests were performed using Prism (GraphPad), p-values are annotated and those marked *
987 were defined as significant.

988
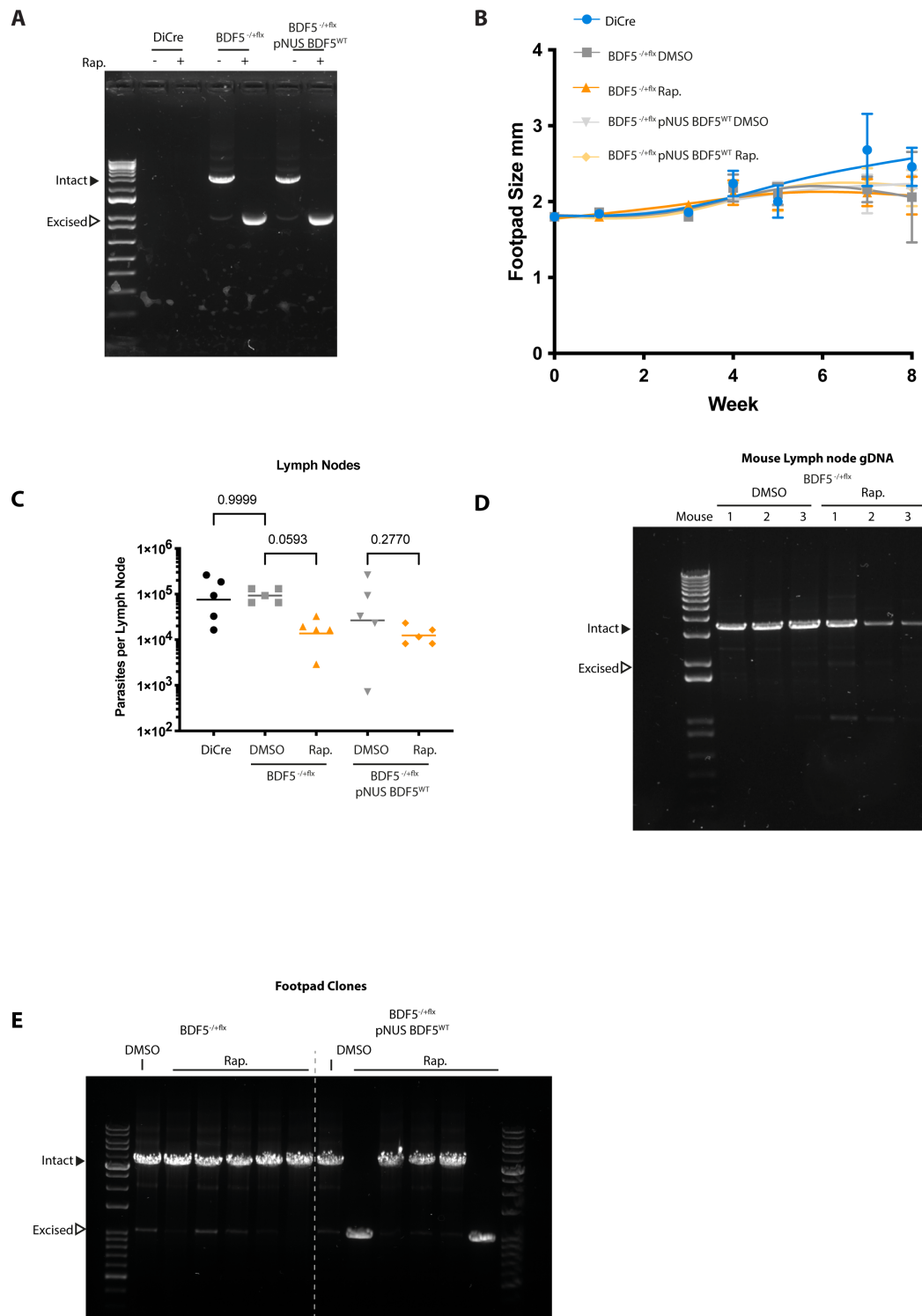
Figure S6: Characterisation of BDF5 using DiCre inducible gene deletion in murine infection. **A.** PCR and agarose gel analysis of stationary phase cultures used to infect mice. **B.** Measurements of footpad lesion size of mice infected with indicated parasite strains. Points and error bars indicate mean ± st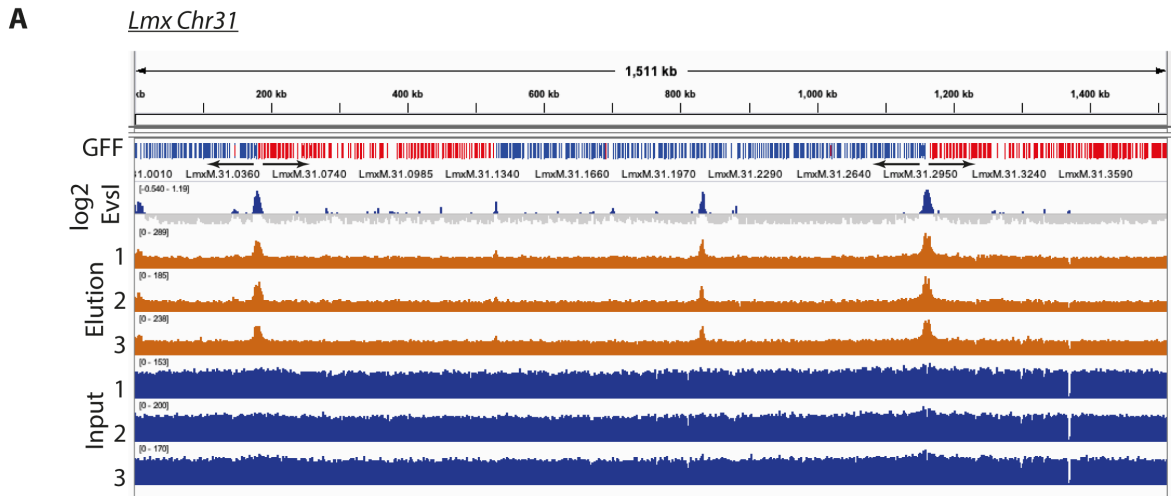andard deviation, N=5. **C.** Parasite burdens from infected mouse popliteal lymph nodes determined by limiting dilution, individual points for each mouse with median values indicated by line. Comparisons of Kruskal-Wallace test with Dunn's correction indicate by lines, associated p-values written above, n=5. **D**. Agarose gel exemplifying PCR analysis of genomic DNA extracted from popliteal lymph nodes of mice
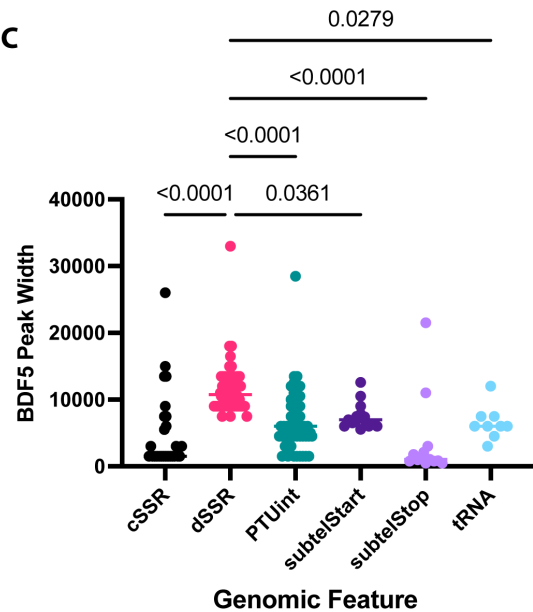
998   infected with the BDF5::6xHA$^{-/+flx}$ cultures that were treated with rapamycin or not, indicating
999   retention of the BDF5 allele at 8-weeks post-infection. **E.** PCR and agarose gel analysis
1000   exemplifying clones surviving as promastigotes following clonogenic assay to detect *BDF5$^{-/+flx}$*
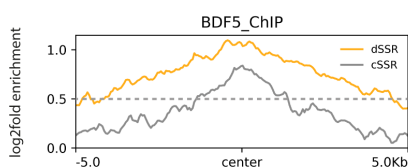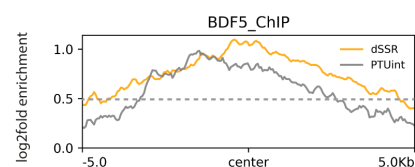1001   allele.
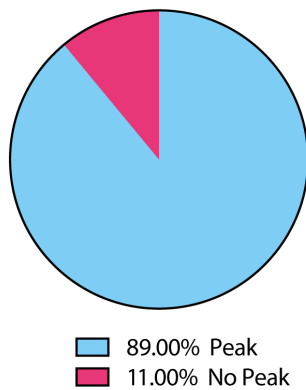
1002
1003   **Figure S7: ChIP-seq analysis of BDF5 distribution on chromatin. A**. Example of IGV genome
1004   browser view of chromosome 31 indicating the genes in polycistronic transcription units
1005   (colour and arrow coded by direction), the read depth for input and eluted sample of the
1006   ChIP-seq (N=3) and the enrichment of BDF5 on a log2 fold scale, GFF (gene feature file)
1007   indicates gene CDS coloured by strand (red+, blue-). **B.** Pie chart indicating the proportion of
1008   SSRs with a BDF5 enriched peak. **C**. BDF5 peak size at different genomic regions as defined by
1009   MACS2 algorithm to call the enriched peaks. cSSR (convergent strand switch region), dSSR
1010   (divergent strand switch region), PTUint (internal PTU peak), subtelStart (subtelomeric peak

1011   consistent with PTU transcriptional start), subtelStop (subtelomeric peak consistent with PTU
1012   transcriptional stop), tRNA (tRNA gene located away from any of the other features). Values
1013   above denote p-value from Kruskal-Wallace test to compare samples. **D**. Metaplot of average
1014   BDF5 fold enrichment at dSSR (n=60) and cSSR (n=40) regions. **E**. Metaplot of BDF5 average
1015   BDF5 fold enrichment at dSSR (n=60) and PTU internal peaks (n=56).
1016
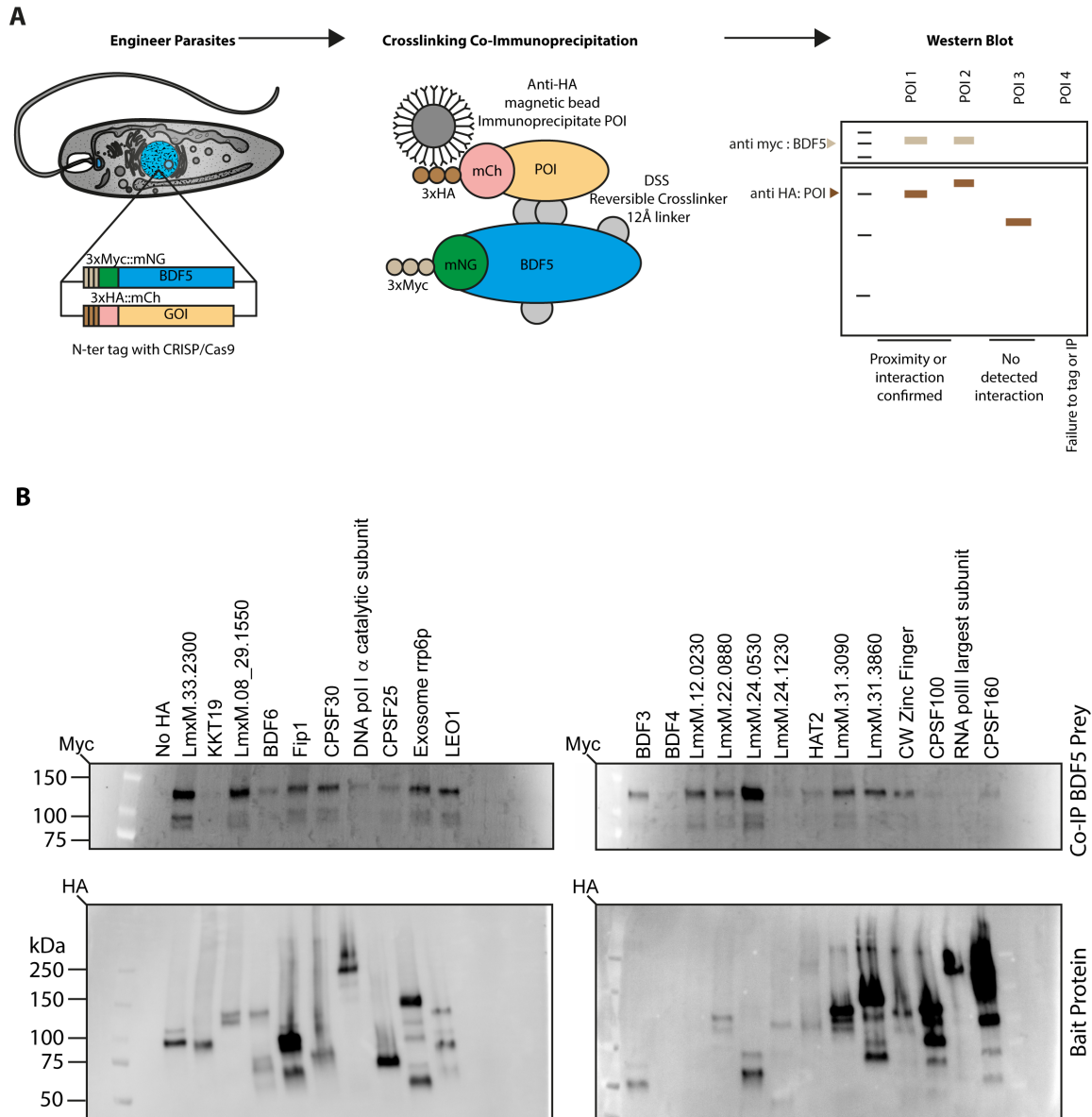
1017
1018   **Figure S8: Co-immunopreciptation analysis of BDF5-proximal proteins. A**. cartoon of
1019   experimental workflow. BDF5-proximal proteins identified by XL-BioID proteins were HA-
1020   tagged in the *LmxT7/Cas9 3xmyc::mNG::BDF5* strain to generate a panel of cell lines containing
1021   both a HA-tagged protein of interest (POI) and myc-tagged BDDF5. **B**. The HA-tagged proteins
1022   were used as bait in an anti-HA immunoprecipitation and co-precipitating (co-IP) myc-tagged
1023   BDF5 protein was is detected using western blot with anti-myc (Upper Panel). Confirmation of
1024   precipitation of the bait protein was confirmed by western blot (lower panel). The presence of
1025   BDF5 co-precipitating with a bait POI confirms the XL-BioID observations as being robust.
1026
1027
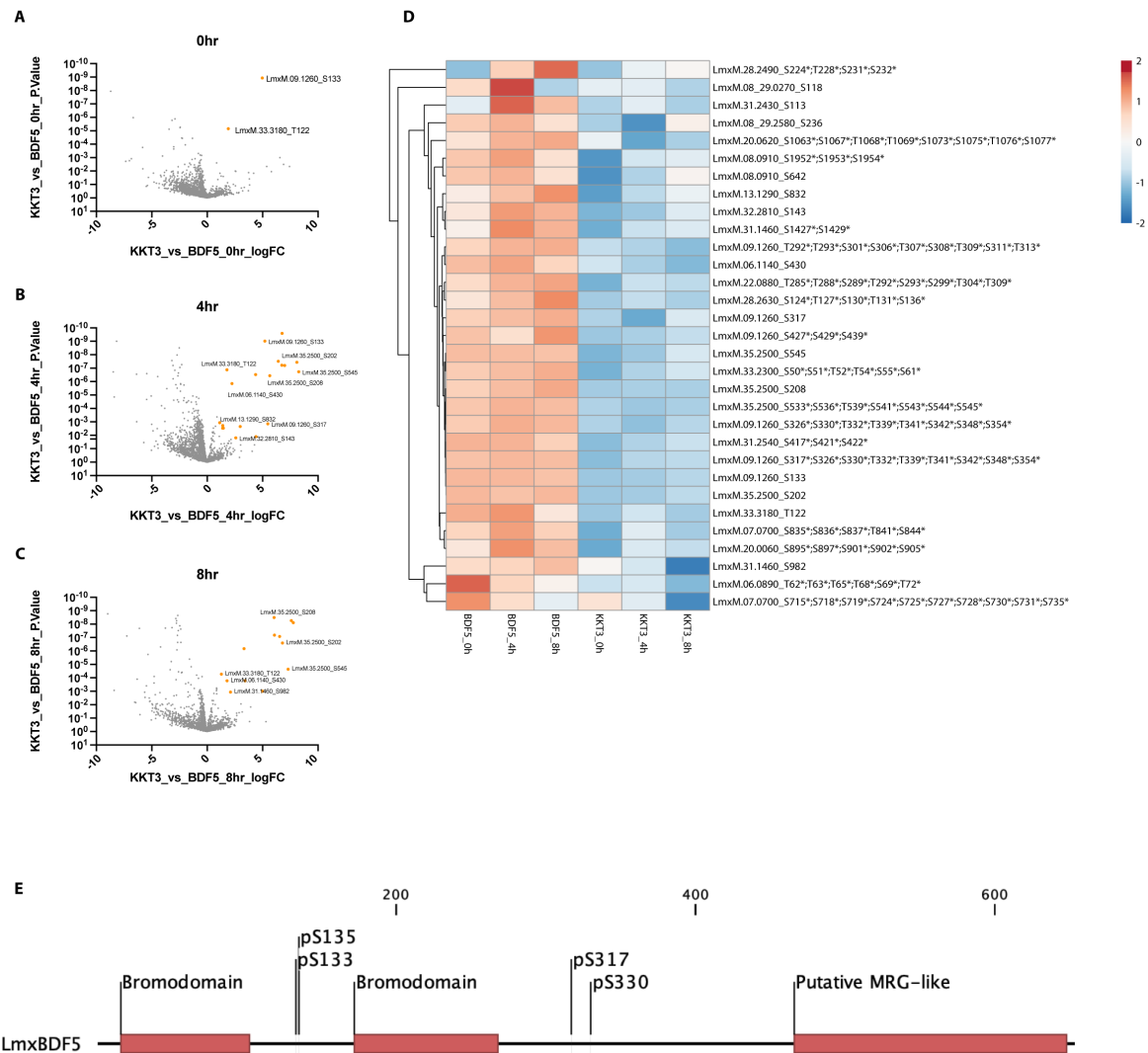
Figure S9: Proximity phosphoproteomic analysis of BDF5 across the cell cycle. A, B and **C.** Volcano plots of phosphopeptide enrichment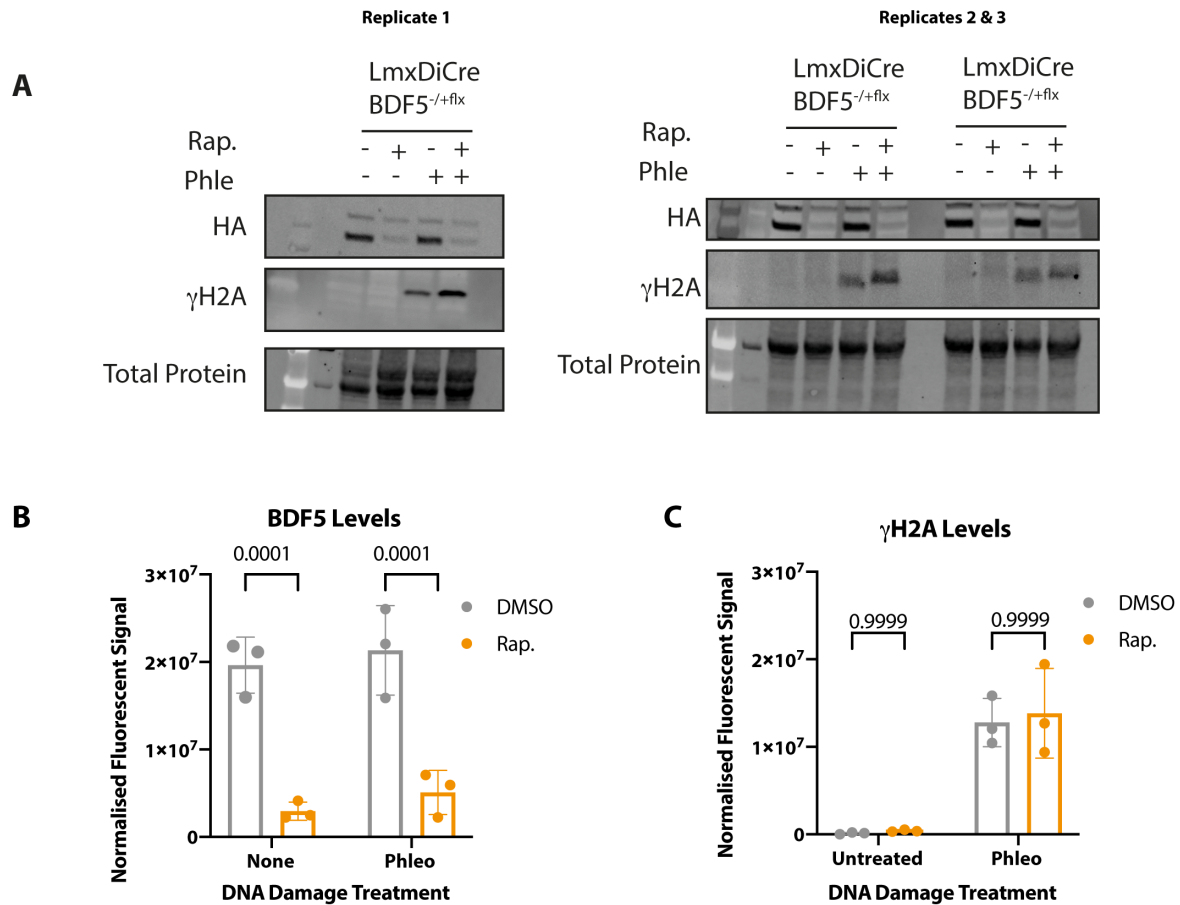 and confidence over 0 h, 4 h and 8 h release from hydroxyurea synchronisation. Ambiguous phosphosite localisations are denoted with a *. **D.** Heatmap of proximal phosphosites represented by median values of 5 replicates after $\log_2+1$ transformation and data centring. Samples depicted are the BDF5 and KKT3 0 h, 4 h and 8 h timepoints.

Figure S10: DNA damage response in BDF5 depleted cells. A. Western blot analysis of cultures treated with DMSO or Rapamycin to delete the floxed allele of *BDF5* in *BDF5^{-/+flx}* for 48 h followed by passaging to 2 x 10^5 cells ml^{-1}l, another 48 h of rapamycin treatment with the final 24 h including or not 1 μg ml^{-1} of phleomycin (Phle). BDF5::6xHA levels and γH2A levels were assessed by Western blot with anti-HA and Anti- γH2A antibodies respectively. (N=3). **B**. Normalised quantification of chemiluminescent signal of BDF5 bands. Data points and bars indicate mean ± SD, N=3. **C**. Normalised quantification of chemiluminescent signal of γH2A bands. Data points and bars indicate mean± SD, data compared by 2-way ANOVA, p-values indicated above. N=3.
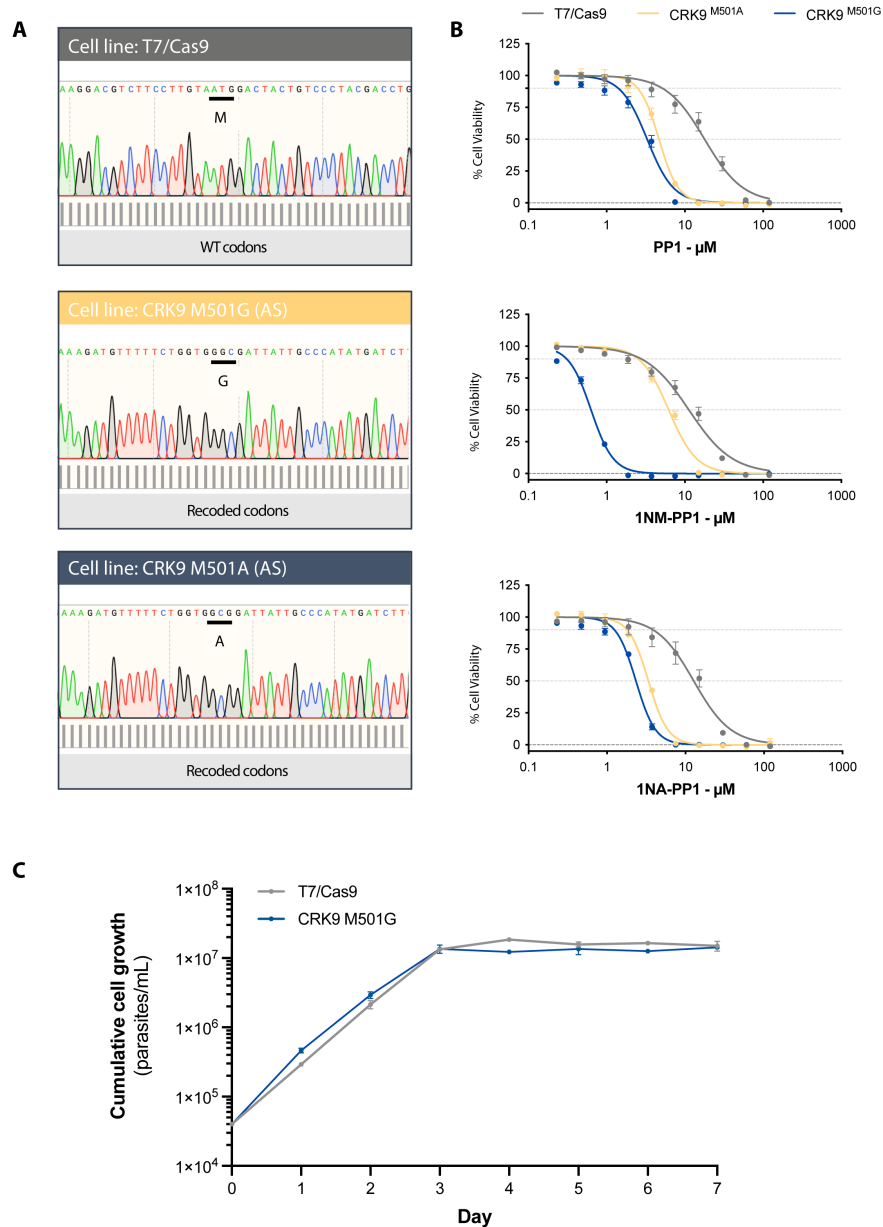
Figure S11: Generation of CRK9 analog-sensitised strains. A. Sanger sequencing of *CRK9* in *L. mexicana T7/Cas9* and precision-edited mutants showing homozygous strains encoding small gatekeeper mutations M501G and M501A. B. Dose-response curves of promastigote cell viability after 72 h treatment in varying concentrations of bulky-kinase inhibitors PP1, 1NM-PP1 and 1NA-PP1, measured by alarm blue method, mean±SD, n=3. C. Growth curve of promastigote cultures of T7.Cas9 and the CRK9[M501A] strain indicating the small gatekeeper residue does not impact growth of promastigotes, mean±SD, n=3.
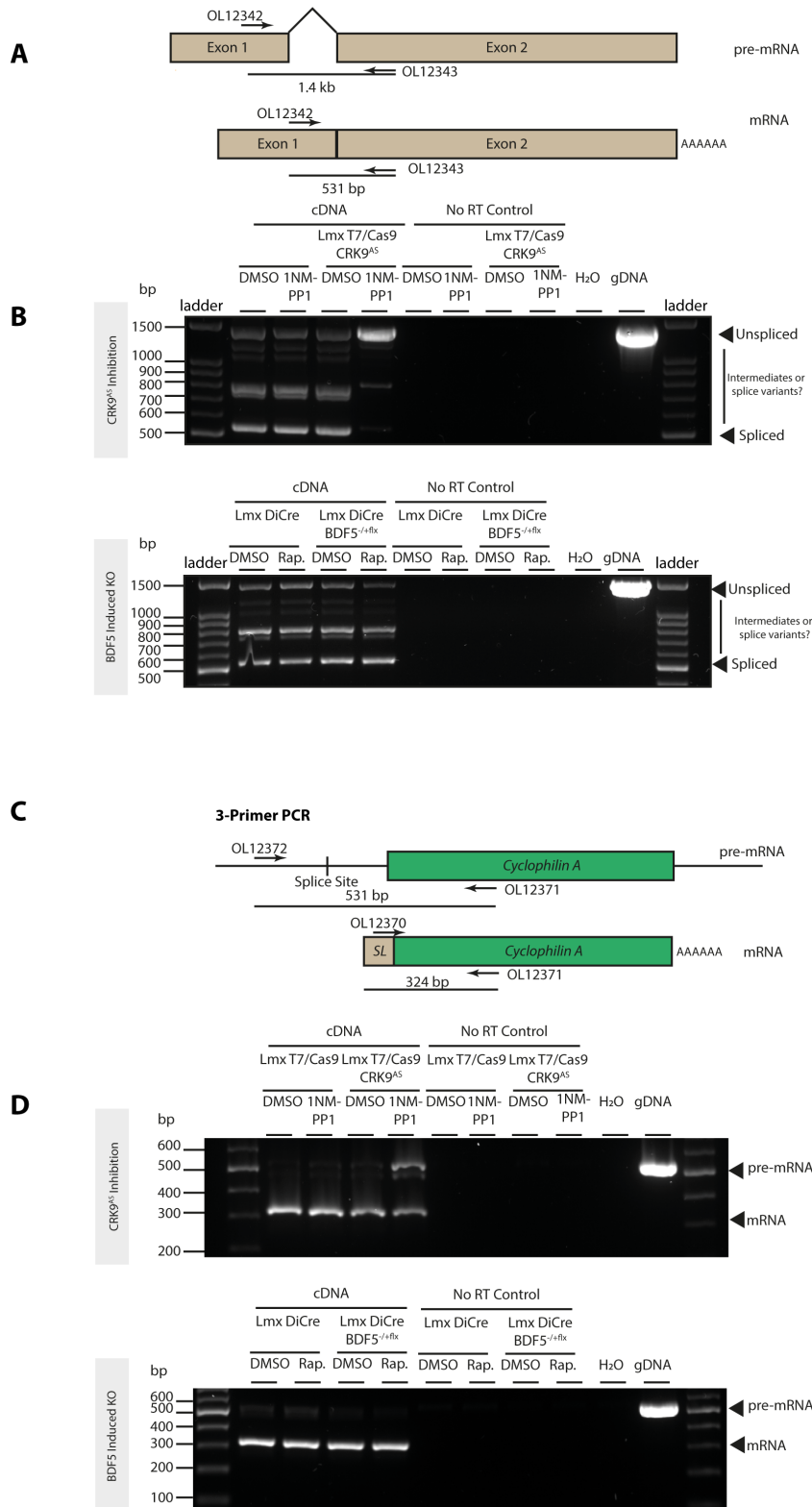
Figure S12: Effect of BDF5 on cis- and trans-splicing of mRNA. A. Cartoon showing the strategy of the RT-PCR assay to detect cis-splicing of polyA-polymerase mRNA (LmxM.08_29.2600) after CRK9 inhibition (a positive control for splicing defects[68]) or BDF5 deletion. Cells were treated with DMSO, Rapamycin or 1NM-PP1. B. Agarose gel of RT-PCR assay to detect cis-splicing of polyA-polymerase mRNA (LmxM.08_29.2600) after CRK9

1062   inhibition or BDF5 deletion. cDNA prepared using random hexamers was used to prime the
1063   assay, thus capturing the pre-mRNA and mRNA. *L. mexicana* T7/Cas9 was used as the control
1064   strain for the CRK9 analog-sensitised strain. Accumulation of the pre-mRNA is only observed
1065   when CRK9^{AS} is inhibited with 1NM-PP1. No-RT controls were included to exclude gDNA
1066   contamination. H_2O indicates a water control to exclude master mix contamination, and
1067   gDNA was used as a positive control to exemplify the unspliced band size. **C**. Cartoon showing
1068   the strategy of the triple-primer RT-PCR assay to detect trans-splicing of Cyclophilin A mRNA
1069   (LmxM.25.0910) after CRK9 inhibition or BDF5 deletion. **D**. Agarose gel of triple-primer RT-
1070   PCR assay to detect trans-splicing of Cyclophilin A mRNA (LmxM.25.0910) after CRK9
1071   inhibition or BDF5 deletion. cDNA prepared using random hexamers was used to prime the
1072   assay, thus capturing the pre-mRNA and mRNA. No-RT controls were included to exclude
1073   gDNA contamination. H_2O indicates a water control to exclude master mix contamination,
1074   and gDNA was used as a positive control to exemplify the unspliced band size. Accumulation
1075   of the pre-mRNA is only observed when CRK9^{AS} is inhibited with 1NM-PP1.
1076
1077

References

1078   **References**

1080   1. Cramer, P. Organization and regulation of gene transcription. *Nature* **573**, 45–54 (2019).

1081   2. Filippakopoulos, P. *et al.* Histone Recognition and Large-Scale Structural Analysis of the Human
1082   Bromodomain Family. *Cell* **149**, 214–231 (2012).

1083   3. Zaware, N. & Zhou, M.-M. Bromodomain biology and drug discovery. *Nat Struct Mol Biol* **26**, 870–879
1084   (2019).

1085   4. Cochran, A. G., Conery, A. R. & Sims, R. J. Bromodomains: a new target class for drug development. *Nat Rev
1086   Drug Discov* **18**, 609–628 (2019).

1087   5. Brand, M. *et al.* Small molecule inhibitors of bromodomain - Acetyl-lysine interactions. *ACS Chemical Biology*
1088   **10**, 22–39 (2015).

1089   6. Wu, Q. *et al.* A chemical toolbox for the study of bromodomains and epigenetic signaling. *Nature
1090   communications* 1–14 (2019) doi:10.1038/s41467-019-09672-2.

1091   7. Burza, S., Croft, S. L. & Boelaert, M. Leishmaniasis. *Lancet* **392**, 951–970 (2018).

1092   8. Clayton, C. Regulation of gene expression in trypanosomatids: living with polycistronic transcription. *Open
1093   biology* **9**, 190072–24 (2019).

1094   9. Wedel, C., Förstner, K. U., Derr, R. & Siegel, T. N. GT-rich promoters can drive RNA pol II transcription and
1095   deposition of H2A.Z in African trypanosomes. *Embo J* **36**, 2581–2594 (2017).

1096   10. Siegel, T. N., Gunasekera, K., Cross, G. A. M. & Ochsenreiter, T. Gene expression in Trypanosoma brucei:
1097   lessons from high-throughput RNA sequencing. *Trends in parasitology* **27**, 434–441 (2011).

1098   11. Pablos, L. M. de *et al.* The mRNA-bound Proteome of Leishmania mexicana: Novel Genetic Insight into an
1099   Ancient Parasite*. *Mol Cell Proteomics* **18**, 1271–1284 (2019).

1100   12. Rogers, M. B. *et al.* Chromosome and gene copy number variation allow major structural change between
1101   species and strains of Leishmania. *Genome research* **21**, 2129–2142 (2011).

1102   13. Dujardin, J.-C., Mannaert, A., Durrant, C. & Cotton, J. a. Mosaic aneuploidy in Leishmania: the perspective
1103   of whole genome sequencing. *Trends in parasitology* **30**, 554–555 (2014).

1104   14. Thomas, S., Green, A., Sturm, N. R., Campbell, D. A. & Myler, P. J. Histone acetylations mark origins of
1105   polycistronic transcription in Leishmania major. *BMC Genomics* **10**, (2009).

1106   15. Kumar, D., Rajanala, K., Minocha, N. & Saha, S. Histone H4 lysine 14 acetylation in Leishmania donovani is
1107   mediated by the MYST-family protein HAT4. *Microbiology (Reading, England)* **158**, 328–337 (2012).

1108   16. Yadav, A., Chandra, U. & Saha, S. Histone acetyltransferase HAT4 modulates navigation across G2/M and
1109   re-entry into G1 in Leishmania donovani. *Scientific Reports* 1–15 (2016) doi:10.1038/srep27510.

1110   17. Kumar, D. & Saha, S. HAT3-mediated acetylation of PCNA precedes PCNA monoubiquitination following
1111   exposure to UV radiation in Leishmania donovani. *Nucleic Acids Research* **43**, 5423–5441 (2015).

18. Chandra, U., Yadav, A., Kumar, D. & Saha, S. Cell cycle stage-specific transcriptional activation of cyclins mediated by HAT2-dependent H4K10 acetylation of promoters in Leishmania donovani. *PLoS Pathogens* **13**, e1006615 (2017).

19. Siegel, T. N. *et al.* Four histone variants mark the boundaries of polycistronic transcription units in Trypanosoma brucei. *Genes & Development* **23**, 1063–1076 (2009).

20. Kraus, A. J. *et al.* Distinct roles for H4 and H2A.Z acetylation in RNA transcription in African trypanosomes. *Nature communications* 1–15 (2020) doi:10.1038/s41467-020-15274-0.

21. Zhang, N. *et al.* Landscapes of Protein Posttranslational Modifications of African Trypanosoma Parasites. *iScience* **23**, 101074 (2020).

22. Staneva, D. P. *et al.* A systematic analysis of Trypanosoma brucei chromatin factors identifies novel protein interaction networks associated with sites of transcription initiation and termination. *Genome Res* gr.275368.121 (2021) doi:10.1101/gr.275368.121.

23. Schulz, D. *et al.* Bromodomain Proteins Contribute to Maintenance of Bloodstream Form Stage Identity in the African Trypanosome. *PLoS Biology* **13**, 1–38 (2015).

24. Alsford, S. *et al.* High-throughput phenotyping using parallel sequencing of RNA interference targets in the African trypanosome. *Genome research* (2011) doi:10.1101/gr.115089.110.

25. Alsford, S. & Horn, D. Cell-cycle-regulated control of VSG expression site silencing by histones and histone chaperones ASF1A and CAF-1b in Trypanosoma brucei. *Nucleic Acids Research* **40**, 10150–10160 (2012).

26. Ritagliati, C. *et al.* Glycosomal bromodomain factor 1 from Trypanosoma cruzi enhances trypomastigote cell infection and intracellular amastigote growth. *The Biochemical journal* **473**, 73–85 (2015).

27. Alonso, V. L., Ritagliati, C., Cribb, P., Cricco, J. A. & Serra, E. C. Overexpression of bromodomain factor 3 in Trypanosoma cruzi (TcBDF3) affects differentiation of the parasite and protects it against bromodomain inhibitors. *FEBS Journal* **283**, 2051–2066 (2016).

28. Alonso, V. L. *et al.* Trypanosoma cruzi bromodomain factor 3 binds acetylated a-tubulin and concentrates in the flagellum during metacyclogenesis. *Eukaryotic Cell* **13**, 822–831 (2014).

29. Villanova, G. V. *et al.* Trypanosoma cruzi bromodomain factor 2 (BDF2) binds to acetylated histones and is accumulated after UV irradiation. *International Journal for Parasitology* **39**, 665–673 (2009).

30. Ivens, A. C. *et al.* The genome of the kinetoplastid parasite, Leishmania major. *Science (New York, N.Y.)* **309**, 436–442 (2005).

31. Zimmermann, L. *et al.* A Completely Reimplemented MPI Bioinformatics Toolkit with a New HHpred Server at its Core. *Journal of molecular biology* **430**, 2237–2243 (2018).

32. Bowman, B. R. *et al.* Multipurpose MRG Domain Involved in Cell Senescence and Proliferation Exhibits Structural Homology to a DNA-Interacting Domain. *Structure* **14**, 151–158 (2006).

33. Zhang, P. *et al.* The MRG domain of human MRG15 uses a shallow hydrophobic pocket to interact with the N-terminal region of PAM14. *Protein Science* **15**, 2423–2434 (2006).

34. Bertram, M. J. & Pereira-Smith, O. M. Conservation of the MORF4related gene family: identification of a new chromo domain subfamily and novel protein motif. *Gene* **266**, 111–121 (2001).

1149   35. Bamborough, P. & Chung, C. Fragments in bromodomain drug discovery. *Medchemcomm* **6**, 1587–1604
1150   (2015).

1151   36. Cho, C. *et al.* Structural basis of nucleosome assembly by the Abo1 AAA+ ATPase histone chaperone.
1152   *Nature communications* 1–13 (2019) doi:10.1038/s41467-019-13743-9.

1153   37. Morozumi, Y. *et al.* Atad2 is a generalist facilitator of chromatin dynamics in embryonic stem cells. *Journal*
1154   *of molecular cell biology* **8**, 349–362 (2016).

1155   38. Gradolatto, A. *et al.* A noncanonical bromodomain in the AAA ATPase protein Yta7 directs chromosomal
1156   positioning and barrier chromatin activity. *Molecular and cellular biology* **29**, 4604–4611 (2009).

1157   39. Goos, C., Dejung, M., Janzen, C. J., Butter, F. & Kramer, S. The nuclear proteome of Trypanosoma brucei.
1158   *PLoS ONE* **12**, e0181884 (2017).

1159   40. Opperdoes, F. R., Butenko, A., Flegontov, P., Yurchenko, V. & Lukeš, J. Comparative Metabolism of Free-
1160   living Bodo saltans and Parasitic Trypanosomatids. *Journal of Eukaryotic Microbiology* 657–678 (2016)
1161   doi:10.1111/jeu.12315.

1162   41. Aurrecoechea, C. *et al.* EuPathDB: the eukaryotic pathogen genomics database resource. *Nucleic Acids*
1163   *Research* **45**, D581–D591 (2017).

1164   42. Beneke, T. *et al.* A CRISPR Cas9 high-throughput genome editing toolkit for kinetoplastids. *Royal Society*
1165   *Open Science* **May**, (2017).

1166   43. Fiebig, M., Kelly, S. & Gluenz, E. Comparative Life Cycle Transcriptomics Revises Leishmania mexicana
1167   Genome Annotation and Links a Chromosome Duplication with Parasitism of Vertebrates. *PLOS Pathogens* **11**,
1168   e1005186-28 (2015).

1169   44. Jones, N. G., Catta-Preta, C. M. C., Lima, A. P. C. A. & Mottram, J. C. Genetically Validated Drug Targets in
1170   Leishmania: Current Knowledge and Future Prospects. *ACS Infectious Diseases* acsinfecdis.7b00244 (2018)
1171   doi:10.1021/acsinfecdis.7b00244.

1172   45. Duncan, S. M. *et al.* Conditional gene deletion with DiCre demonstrates an essential role for CRK3 in
1173   Leishmania mexicana cell cycle regulation. *Molecular Microbiology* **100**, 931–944 (2016).

1174   46. Damianou, A. *et al.* Essential roles for deubiquitination in Leishmania life cycle progression. *Plos Pathog* **16**,
1175   e1008455 (2020).

1176   47. Tetaud, E., Lecuix, I., Sheldrake, T., Baltz, T. & Fairlamb, A. H. A new expression vector for Crithidia
1177   fasciculata and Leishmania. *Mol Biochem Parasit* **120**, 195–204 (2002).

1178   48. Philpott, M. *et al.* Assessing cellular efficacy of bromodomain inhibitors using fluorescence recovery after
1179   photobleaching. *Epigenet Chromatin* **7**, 14 (2014).

1180   49. Umehara, T. *et al.* Structural Basis for Acetylated Histone H4 Recognition by the Human BRD2
1181   Bromodomain*. *J Biol Chem* **285**, 7610–7618 (2010).

1182   50. Santos, R. E. R. S. *et al.* A DiCre recombinase-based system for inducible expression in Leishmania major.
1183   *Molecular and biochemical parasitology* **216**, 45–48 (2017).

1184   51. Geoghegan, V., Jones, N. G., Dowle, A. & Mottram, J. C. Protein kinase signalling at
1185   the Leishmania kinetochore captured by XL-BioID. *bioRxiv* (2021)
1186   doi:https://doi.org/10.1101/2021.07.08.451598.

1187   52. Roux, K. J., Kim, D. I., Raida, M. & Burke, B. A promiscuous biotin ligase fusion protein identifies proximal
1188   and interacting proteins in mammalian cells. *Journal of cell biology* **196**, 801–810 (2012).

1189   53. Baker, N. *et al.* Systematic functional analysis of Leishmania protein kinases identifies regulators of
1190   differentiation or survival. *Nat Commun* **12**, 1244 (2021).

1191   54. Garcia-Silva, M. *et al.* Identification of the centromeres of Leishmania major: revealing the hidden pieces.
1192   *Embo Rep* **18**, 1968–1977 (2017).

1193   55. Zhao, X. SUMO-Mediated Regulation of Nuclear Functions and Signaling Processes. *Mol Cell* **71**, 409–418
1194   (2018).

1195   56. Liao, S., Wang, T., Fan, K. & Tu, X. The small ubiquitin-like modifier (SUMO) is essential in cell cycle
1196   regulation in Trypanosoma brucei. *Exp Cell Res* **316**, 704–715 (2010).

1197   57. Mi, J. *et al.* Crystal structure of an ENT domain from Trypanosoma brucei. *Biochem Bioph Res Co* **505**, 755–
1198   760 (2018).

1199   58. Chavali, G. B. *et al.* Crystal Structure of the ENT Domain of Human EMSY. *J Mol Biol* **350**, 964–973 (2005).

1200   59. Reynolds, D. *et al.* Regulation of transcription termination by glucosylated hydroxymethyluracil, base J, in
1201   Leishmania major and Trypanosoma brucei. *Nucleic Acids Research* **42**, 9717–9729 (2014).

1202   60. Briggs, E., Hamilton, G., Crouch, K., Lapsley, C. & McCulloch, R. Genome-wide mapping reveals conserved
1203   and diverged R-loop activities in the unusual genetic landscape of the African trypanosome genome. *Nucleic*
1204   *Acids Res* **46**, gky928- (2018).

1205   61. Marques, C. A., Dickens, N. J., Paape, D., Campbell, S. J. & Mcculloch, R. Genome-wide mapping reveals
1206   single-origin chromosome replication in Leishmania, a eukaryotic microbe. *Genome Biology* 1–12 (2015)
1207   doi:10.1186/s13059-015-0788-9.

1208   62. Anderson, B. A. *et al.* Kinetoplastid-specific histone variant functions are conserved in Leishmania major.
1209   *Molecular and biochemical parasitology* **191**, 53–57 (2013).

1210   63. Katiyar, S. *et al.* Lapatinib-binding protein kinases in the african trypanosome: identification of cellular
1211   targets for kinase-directed chemical scaffolds. *PLoS ONE* **8**, e56150 (2013).

1212   64. Briggs, E. *et al.* Trypanosoma brucei ribonuclease H2A is an essential R-loop processing enzyme whose loss
1213   causes DNA damage during transcription initiation and antigenic variation. *Nucleic Acids Res* **47**, 9180–9197
1214   (2019).

1215   65. Kim, J. J. *et al.* Systematic bromodomain protein screens identify homologous recombination and R-loop
1216   suppression pathways involved in genome integrity. *Gene Dev* **33**, 1751–1774 (2019).

1217   66. Floyd, S. R. *et al.* The bromodomain protein Brd4 insulates chromatin from DNA damage signalling. *Nature*
1218   **498**, 246–250 (2013).

1219   67. Glover, L. & Horn, D. Trypanosomal histone γH2A and the DNA damage response. *Mol Biochem Parasit*
1220   **183**, 78–83 (2012).

1221   68. Gosavi, U., Srivastava, A., Badjatia, N. & Günzl, A. Rapid block of pre-mRNA splicing by chemical inhibition
1222   of analog-sensitive CRK9 in Trypanosoma brucei. *Molecular Microbiology* **113**, 1225–1239 (2020).

1223 69. Jha, P. K., Khan, M. I., Mishra, A., Das, P. & Sinha, K. K. HAT2 mediates histone H4K4 acetylation and affects
1224 micrococcal nuclease sensitivity of chromatin in Leishmania donovani. *PLoS ONE* **12**, e0177372 (2017).

1225 70. Oss, S. B. V., Cucinotta, C. E. & Arndt, K. M. Emerging Insights into the Roles of the Paf1 Complex in Gene
1226 Regulation. *Trends Biochem Sci* **42**, 788–798 (2017).

1227 71. Wang, R. *et al.* Uncovering BRD4 hyperphosphorylation associated with cellular transformation in NUT
1228 midline carcinoma. *Proc National Acad Sci* **114**, E5352–E5361 (2017).

1229 72. Wang, R., Yang, J. F., Ho, F., Robertson, E. S. & You, J. Bromodomain-Containing Protein BRD4 Is
1230 Hyperphosphorylated in Mitosis. *Cancers* **12**, 1637 (2020).

1231 73. Peng, D. & Tarleton, R. Short Paper EuPaGDT : a web tool tailored to design CRISPR guide RNAs for
1232 eukaryotic pathogens. 1–7 (2017) doi:10.1099/mgen.0.000033.

1233 74. Sunter, J. D. *et al.* Leishmania flagellum attachment zone is critical for flagellar pocket shape, development
1234 in the sand fly, and pathogenicity in the host. *Proc National Acad Sci* **116**, 201812462 (2019).

1235 75. Kelley, L. A., Mezulis, S., Yates, C. M., Wass, M. N. & Sternberg, M. J. E. The Phyre2 web portal for protein
1236 modeling, prediction and analysis. *Nat Protoc* **10**, 845–858 (2015).

1237
1238